

Aus der
Medizinischen Klinik und Poliklinik II
Klinikum der Ludwig-Maximilians-Universität München



The role of bile salts in cholestatic liver fibrosis

Dissertation
zum Erwerb des Doktorgrades der Medizin
an der Medizinischen Fakultät der
Ludwig-Maximilians-Universität zu München

vorgelegt von
Jingguo Li

aus
Guizhou, P.R. China

Jahr
2024

Mit Genehmigung der Medizinischen Fakultät der
Ludwig-Maximilians-Universität München

Erstes Gutachten: Priv. Doz. Dr. Simon Hohenester
Zweites Gutachten: Priv. Doz. Dr. Andreas Kremer
Drittes Gutachten: Prof. Dr. Alexander Dietrich

Promovierter Mitbetreuer: Priv. Doz. Gerald Denk
Dekan: Prof. Dr. med. Thomas Gudermann

Tag der mündlichen Prüfung: 14.05.2024

Table of content

Table of content.....	3
Zusammenfassung (Deutsch):.....	5
Abstract (English):	7
List of figures.....	9
List of tables	10
List of abbreviations	11
1. Introduction to the liver in health and disease	13
1.1 Liver function in health	13
1.2 Liver cirrhosis and consequences of deteriorated liver function.....	13
1.3 Chronic cholestatic liver disease	14
1.3.1 Pathogenesis of cirrhosis in CLD	16
1.3.2 Role of bile salt-induced activation of hepatic stellate cells in fibrogenesis ..	19
2. Aims	22
3. Material and Methods	23
3.1 Cell culture.....	23
3.2 Viability assay	23
3.3 pHi measurement in LX2	24
3.4 Measurement of bile salt accumulation in LX2.....	24
3.5 DNA quantification assay.....	25
3.6 Reverse-transcription quantitative polymerase chain reaction (RT-qPCR)	25
3.7 Western Blotting	26
3.8 Na ⁺ /H ⁺ activity measurement	27
3.9 Animals	27
3.10 Bile acid analysis	29
3.11 Serum analysis.....	29
3.12 Liver histology	29

3.13	Immunohistochemistry	30
3.14	Statistical analysis	30
4.	Results	32
4.1	GCDC feeding induces a humanized bile salt pool in BDL and CCl ₄ mouse models.....	32
4.2	Humanized bile salt pool aggravates liver fibrosis in mouse models of CLD...35	
4.3	CDC, but not GCDC, induces activation of HSC in standard cell culture conditions	40
4.4	Activation of HSC by (G)CDC is crucially determined by extracellular pH.....	42
4.5	Inhibition of sodium-hydrogen exchanger in HSC leads to intracellular acidification, prevent bile salt uptake and (G)CDC-induced HSC activation...47	
4.6	(G)CDC-induced HSCs activation is ameliorated by proton pump inhibitors targeting NHE and vacuolar(v)-H ⁺ -ATPase.....	51
4.7	Pantoprazole prevents liver fibrosis in the DDC-diet model of chronic cholestasis.....	56
4.8	Pantoprazole prevents liver fibrosis in the BDL model of acute cholestasis .59	
5.	Discussion	63
5.1	Conclusion.....	68
5.2	Outlook.....	68
	References	69
	Acknowledgements.....	74
	Affidavit	75
	List of publications	76

Zusammenfassung (Deutsch):

Das Krankheitsbild der Leberzirrhose geht mit erheblicher Morbidität und Mortalität einher, und die derzeitigen Behandlungsmöglichkeiten für diese Lebererkrankung im Endstadium konzentrieren sich auf das Management von Komplikationen, während echte Therapieoptionen zur Behandlung der Zirrhose selbst fehlen. Die Sterblichkeitsraten durch Leberzirrhose sind in den letzten Jahrzehnten daher weiter gestiegen, und das trotz der Fortschritte, die z. B. bei der Behandlung von Virushepatitis erreicht wurden. Somit verbleibt im Bereich chronischer Lebererkrankungen ein hoher Bedarf an weiteren Therapieoptionen. Hauptursachen für eine Leberzirrhose sind Virushepatitis, alkoholische Lebererkrankungen und nichtalkoholische Lebererkrankungen. Eine häufige weitere Ursache einer Leberzirrhose sind chronisch cholestatische Lebererkrankungen (CLD). CLD sind durch die systemische und hepatische Akkumulation von Gallensalzen gekennzeichnet, welcher eine hohe Bedeutung für die Fibrogenese bei CLD beigemessen wird. Die Mechanismen, die der Cholestase-induzierten Fibrogenese zugrunde liegen sind jedoch noch nicht vollständig verstanden.

Wir hatten in früheren Arbeiten gezeigt, dass die Humanisierung des Gallensalzpools im Mausmodell der hepatozellulären Cholestase zu einer fortgeschritteneren Leberfibrose führte, was auf einen Einfluss der Gallensalzzusammensetzung oder einzelner Gallensalze auf die Leberfibrogenese hindeutet. Aktuell untersuchten wir daher *in vivo* weiter die Rolle des menschlichen Gallensalzpools für die Entstehung der Leberfibrose in verschiedenen Krankheitsmodellen.

Als Mechanismus der mit Cholestase verbundenen Fibrogenese wurde bereits früher die direkte Aktivierung hepatischer Sternzellen

(HSC) durch akkumulierende Gallensalze vermutet. In anderen Zelltypen wurde der extrazelluläre pH als Modulator der Gallensalz-induzierten Signalgebung identifiziert und könnte bei HSC pathophysiologisch relevant sein, wenn man bedenkt, dass sie sich in einer bekanntermaßen leicht sauren ‚microenvironment‘, dem (perisinusoidalen) Disse-Raum, befinden. Daher untersuchten wir *in vitro* den Einfluss des extrazellulären pH auf den Gallensalzeintritt, die HSC-Aktivierung und die extrazelluläre Kollagenablagerung in der HSC-Zelllinie LX2. Modulatoren des intrazellulären pH-Werts, der Protonenpumpenhemmer (PPI) Pantoprazol (PPZ), der Na⁺/H⁺-Austauscher (NHE)-Hemmer Amilorid und der vakuoläre ATPase-Hemmer Bafilomycin A1, wurden auf ihre Fähigkeit getestet, den Eintritt von Gallensalzen und die HSC-Aktivierung zu verhindern. Schließlich wurde PPZ im DDC-Diätmodell der cholestatischen Leberfibrose eingesetzt.

Wir fanden heraus, dass die GCDC-Fütterung den Gallensalzpool humanisierte und die Leberfibrose sowohl bei cholestatischen als auch bei nicht-cholestatischen Mausmodellen der Leberfibrose verschlimmerte. *In vitro* erhöhte ein leicht saurer extrazellulärer pH-Wert (pHe 7.3) die intrazelluläre Gallensalzanreicherung in LX2 und war eine Voraussetzung für die Gallensalz-induzierte Aktivierung und Kollagenablagerung. PPZ führte über die Hemmung der NHE-Aktivität zu einer Senkung des intrazellulären pH-Werts (pHi) und verhinderte die Gallensalz-induzierte Aktivierung von LX2. Ähnliche Ergebnisse wurden nach pHi-Modulation mit Amilorid und Bafilomycin A1 gefunden. *In vivo* linderte PPZ (5 mg/kg) die cholestatische Leberfibrose.

Zusammenfassend lässt sich sagen, dass 1) ein humanisierter Gallensalzpool sowohl bei cholestatischer als auch bei nicht-cholestatischer Leberfibrose fibrogener ist als der Gallensalzpool der Maus; 2) die direkte, durch Gallensalze induzierte Aktivierung von

HSCs von dem leicht sauren ‚microenvironment‘ des perisinusoidalen Raums abhängt und 3) die Modulation des pHi bei HSC die profibrogenen Signale bei Cholestase positiv beeinflussen kann. Daher verdienen pharmakologische Wirkstoffe, die speziell auf HSCs zur Modulation des pHi abzielen, möglicherweise weitere Untersuchung als Behandlungsoption bei CLD.

Abstract (English):

Liver Cirrhosis is associated with marked morbidity and mortality, and current treatment options in this end-stage liver disease are scarce. As a result, mortality rates in liver cirrhosis have increased over the past decades and despite the advances made e.g. in the treatment of viral hepatitis, remains an area of high unmet medical need. Major causes of liver cirrhosis are viral hepatitis, alcoholic liver disease and non-alcoholic liver disease. A frequent additional cause of liver cirrhosis are chronic cholestatic liver diseases (CLD). CLD are characterized by the hepatic accumulation of bile salts, which are believed to be a main driver of fibrogenesis. However, mechanisms underlying cholestasis-induced fibrogenesis in cholestasis remain incompletely understood.

We had previously shown that humanization of the bile salt pool led to more advanced liver fibrosis in mouse model of hepatocellular cholestasis, hinting towards an influence of bile salt composition or individual bile salts for liver fibrogenesis. Here, we investigated further *in vivo*, into role of the human bile salt pool for the development of liver fibrosis in various disease models.

As a component of fibrogenesis associated with cholestasis, direct activation of hepatic stellate cells (HSC) by accumulating bile salts

has been suggested. In this context, extracellular pH has been identified as a modulator in bile salt signaling in other cell types and may be pathophysiologically relevant in HSC, considering that they reside in a microenvironment known to be slightly acidic, the (perisinusoidal) space of Disse. Therefore, *in vitro*, we evaluated the influence of extracellular pH on bile salt entry, HSC activation and extracellular collagen deposition in the HSC cell line LX2. Modulators of intracellular pH, the proton pump inhibitors (PPI) pantoprazole (PPZ), Na⁺/H⁺ exchanger (NHE) inhibitor amiloride and vacuolar-ATPase inhibitor bafilomycin A1, were tested for their ability to prevent bile salt entry and HSC activation. Lastly, PPZ was employed in the DDC-diet model of cholestatic liver fibrosis.

We found that GCDC feeding humanized the bile salt pool and aggravated liver fibrosis both cholestatic and non-cholestatic mouse models of liver fibrosis. *In vitro*, slightly acidic extracellular pH (pHe 7.3) enhanced intracellular bile salt accumulation in LX2 and was a prerequisite to bile salt-induced activation and collagen deposition. PPZ led to a decrease in intracellular pH (pHi) via inhibition of NHE activity and prevented bile salt-induced activation of LX2. Similar results were found after pHi modulation with amiloride and bafilomycin A1. *In vivo*, PPZ (5 mg/kg) ameliorated cholestatic liver fibrosis.

In conclusion, 1) a human bile salt pool is more fibrogenic than the murine bile salt pool in both cholestatic and non-cholestatic liver fibrosis; 2) direct bile salt-induced activation of HSC may depend on the slightly acidic microenvironment of the perisinusoidal space; 3) modulation of pHi in HSC may ameliorate pro-fibrogenic signals in liver disease. Thus, pharmacological agents specifically targeting HSCs to modulate pHi may deserve further investigation as treatment options in CLD.

List of figures

Figure 1 Numbers and age-standardized rates of cirrhosis-associated deaths globally during 1990-2017.....	14
Figure 2 Different etiologies of cholestatic liver diseases impact different structures in the biliary tree	16
Figure 3 Overview of fibrogenesis in cholestatic liver disease.	18
Figure 4 The liver sinusoidal unit.	21
Figure 5 GCDC feeding humanized the bile salt pool in the mouse model of BDL. ..	33
Figure 6 GCDC feeding humanized the bile salt pool in the mouse model of CCl ₄ ..	34
Figure 7 GCDC feeding-induced human-like bile salt pool aggravated liver fibrosis in a BDL mouse model	38
Figure 8 GCDC feeding-induced human-like bile salt pool aggravated liver fibrosis in a CCl ₄ mouse model	39
Figure 9 GCDC, unlike CDC, is unable to activate LX2 cells in standard culture conditions.	41
Figure 10 Extracellular pH determines intracellular bile salt accumulation and bile salt-induced activation of LX2 cells.....	46
Figure 11 PPZ inhibits Na ⁺ /H ⁺ exchanger to lower pHi and is associated with protection against bile salt entry and GCDC-induced pro-fibrogenic activation in LX2.	49
Figure 12 CDC-induced activation of LX2 is ameliorated by PPZ, associated with pHi alteration.	50
Figure 13 Amiloride and bafilomycin A1 alter pHi and inhibit GCDC-induced activation of LX2.	54
Figure 14 Amiloride and bafilomycin A1 alter pHi and inhibit CDC-induced activation of LX2.	56
Figure 15 PPZ ameliorates DDC-induced cholestatic liver fibrosis in mice.	58
Figure 16 PPZ ameliorates BDL-induced cholestatic liver fibrosis in mice.....	62

List of tables

Table 1 Primers Information for Reverse-Transcription Quantitative Polymerase	
Chain Reaction Gene name	26

List of abbreviations

ALT	Alanine aminotransferase
AST	Aspartate aminotransferase
α SMA	α -smooth muscle actin
BDL	Bile duct ligation
Bafil A1	Bafilomycin A1
BSEP	Bile salt export pump
CCl ₄	Carbon tetrachloride
CDC	Chenodeoxycholate
CLD	Cholestatic liver disease
CLF	Cholyl-Lysyl-Fluorescein
DDC	3,5-Diethoxycarbonyl-1,4-Dihydrocollidine
GCDC	Glycochenodeoxycholate
GC	Glycocholate
GDC	Glycodeoxycholate
HSCs	Hepatic stellate cells
MAPK	Mitogen-activated protein kinase
MC	Muricholate
NTCP	Sodium taurocholate co-transporting polypeptide
NHE	Na ⁺ /H ⁺ exchanger
OATP	Organic anion transporting polypeptide

PFIC	Progressive familial intrahepatic cholestasis
PBC	Primary biliary cholangitis
pHe	Extracellular pH
pHi	Intracellular pH
PPZ	Pantoprazole
PPI	Proton pump inhibitor
PSC	Primary sclerosing cholangitis
TBIL	Total bilirubin
TGR5	G-protein-coupled receptor
T α MC	Tauro- α -muricholate
T β MC	Tauro- β -muricholate
T ω MC	Tauro- ω -muricholate
TC	Taurocholate
TCDC	Taurochenodeoxycholate
TDC	Taurodeoxycholate
TGF- β	Transforming growth factor- β
TGR5	G-protein-coupled receptor
v-ATPase	Vacuolar ATPase

1. Introduction to the liver in health and disease

1.1 Liver function in health

Liver, the largest internal organ in human body, plays a critical role in numerous physiological processes. This includes protein synthesis, elimination of internal and external toxins via bile, clearance of toxins from blood, amino acid metabolism, regulation of blood coagulation, immune balance, storage of vitamins energy storage and glucose metabolism, many of which are vital to human health¹. All processes are tightly regulated in health, and disturbance of any of these processes may result in detrimental health conditions.

1.2 Liver cirrhosis and consequences of deteriorated liver function

Liver cirrhosis describes the replacement of healthy liver tissue by functionally inactive scar tissue. It can be the consequence of various types of (chronic) liver diseases and conditions, such as non-alcoholic fatty liver disease, chronic hepatitis B or C infection, harmful alcohol consumption, (genetically determined) iron or copper overload, cholestatic diseases and liver autoimmune disease². After a long period of liver damage that triggers inflammation and fibrogenesis, normal liver parenchymal is replaced by dense fibrotic tissue and diffuse regenerative nodules, resulting in a gradual loss of liver function³. Liver cirrhosis is associated with high morbidity and mortality, leading to roughly one million deaths annually. Thus, it ranks the 11th most common cause of death worldwide⁴. Clinically, liver cirrhosis is diagnosed on the basis of multiple factors and can be accompanied in late stages with various complications, such as portal hypertension & variceal bleeding, hepatic synthetic dysfunction, ascites, hepatic encephalopathy, hepatocellular carcinoma. At this moment, there is no effective treatment for cirrhosis, except for liver transplantation^{2,3}. However, challenges, such as the complexity of surgical technique, immuno-

suppression and the shortage of liver sources, hinder patients to easily benefit from liver transplantation⁵. During 1990-2017, cirrhosis-led deaths increased from 0.89 million to 1.32 million globally (Figure 1). Thus, there is dire unmet medical need for improved therapies to halt progression of liver disease to liver cirrhosis.

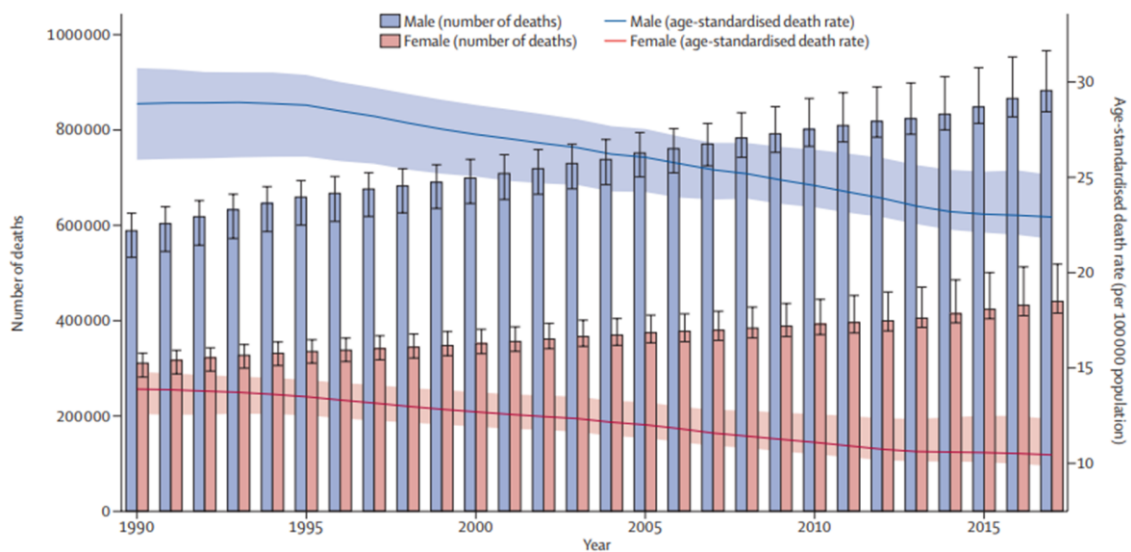


Figure 1. Numbers and age-standardized rates of cirrhosis-associated deaths globally during 1990-2017. Cirrhosis-led deaths totally increased from 0.89 million to 1.32 million globally. (Taken from the Global Burden of Disease Study 2017 Cirrhosis collaborators⁶)

1.3 Chronic cholestatic liver disease

Cholestasis is a pathological state in which bile-bound elimination of toxins and other substances is disturbed, associated with an accumulation of these substances in the liver and systemically. Cholestasis may occur acutely, e.g. due to biliary obstruction by gallstones, or may occur chronically, in a diverse group of diseases summarized as chronic cholestatic liver disease (CLD)⁷. CLD is a pathophysiolog-

ically rather diverse group of liver diseases, encompassing a spectrum of inflammation and damage of large bile ducts, such as primary sclerosing cholangitis (PSC), destruction of microscopically small bile ducts, such as primary biliary cholangitis (PBC), and conditions with defects in bile generation, such as the inborn cholestatic syndromes progressive familial intrahepatic cholestasis (PFIC) (Figure 2). Despite the mostly slow progress of CLD with often merely mild hepatic dysfunction, in lack of curative treatment option, it may progress to liver fibrosis and cirrhosis, eventually necessitating for liver transplantation⁸. Currently, general understanding of CLD epidemiology is limited. The most abundant of these diseases, PBC has a prevalence and incidence of 35/100,000 and 2-3/100,000, respectively. In Germany, roughly 30.000 patients are considered to be affected⁹.

Only in PBC has a pharmacological therapy successfully been established. In all other CLD, effective, evidence-based pharmacological treatment options are lacking. This explains the continuous unmet need to better understand the pathophysiology behind CLD-induced liver fibrosis and to exploration new therapy strategies.

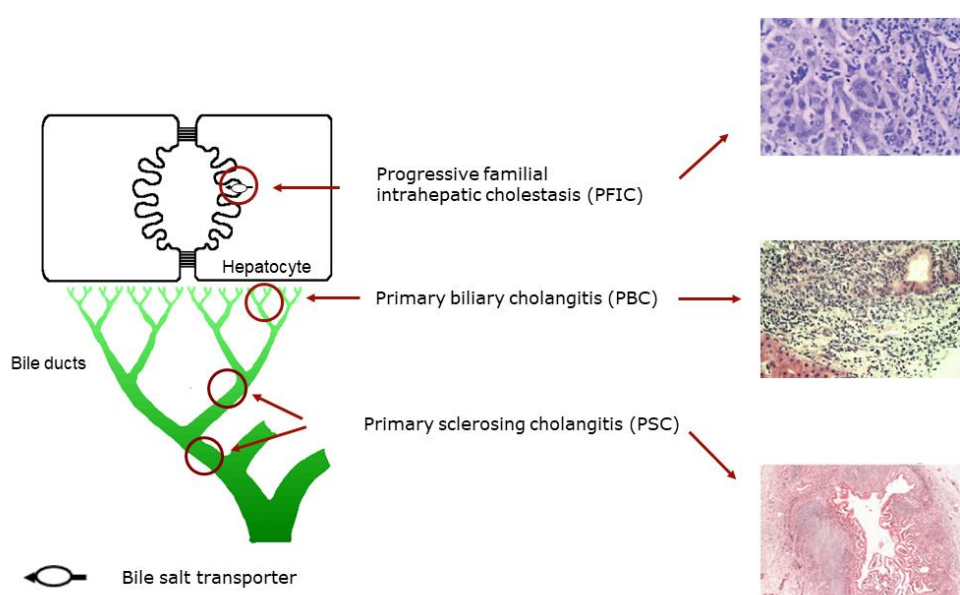


Figure 2. Different etiologies of cholestatic liver diseases impact different structures in the biliary tree. (Left panel) PFIC is led by defects in bile salt transporters; PBC is led by destruction of microscopically small bile ducts; PSC is led by damage on large small ducts. (Right panel) Representative histology stainings of PFIC, PBC and PSC (Taken from Gideon M. Hirschfield et al. and Mohamed A. El-Guindi et al. ^{10,11})

1.3.1 Pathogenesis of liver cirrhosis in CLD

The pathogenesis of the various CLD is very intricate, involving - among others - genetic variants, external and internal toxins, or aberrations in the immune system. During the long-term course of disease, all may ultimately progress to liver cirrhosis. Despite their varying pathogenetic pathways, however, CLDs share the systemic and hepatic accumulation of bile salts^{12,13}. For example, PBC patients were found a 20-fold increase of systemic bile salt levels in advanced stages¹⁴.

Accumulating bile salts have been implicated in fibrogenesis in CLD, a hypothesis that has been widely accepted since the 1970s^{12,15}, and up to today, therefore, bile salt accumulation is considered as a driving force of fibrosis in CLD¹⁶⁻¹⁹. Mechanisms of fibrogenesis in CLD is summarized in Figure 3. Mechanisms driving bile-salt induced fibrogenesis may involve hepatocellular apoptosis and injury^{18,20-25} with uptake of apoptotic bodies or DNA derived from dying hepatocytes by hepatic stellate cells (HSC) and subsequent activation²⁶⁻²⁹. However, these proposed mechanisms have mainly been identified *in vitro*, have hardly been reproduced and have hardly been translated into *in vivo* models.

In addition, in currently widely used animal models of cholestasis, such as *multidrug resistance protein 2* knockout mice and bile duct ligation, liver fibrosis may be induced independently of accumulating bile salts, by biliary damage and inflammation³⁰. In the purely cholestatic mouse model of the bile salt export pump (BESP)-knockout, however, bile salt accumulation failed to induce liver fibrosis in mice³¹. Therefore, it has been doubted that accumulating bile salts in cholestasis truly lead to fibrosis³². These contradictory findings might partly be explained by different bile salt pools in humans and mice. Mice present a highly hydrophilic bile salt pool, where muricholate (MC) takes the most, while human bile salt pool is more hydrophobic, where chenodeoxycholate (CDC) predominates¹⁹. We have previously demonstrated that the presence of glycol-conjugated CDC (GCDC) is crucial for development of liver fibrosis in a *in vivo* model of hepatocellular cholestasis³⁰, which was the first *in vivo* evidence for the concept that hydrophobic bile salts accumulating in CLD promote liver fibrosis.

In summary, the pro-fibrogenic mechanisms associated with bile salt accumulation in CLD still remain incompletely characterized.

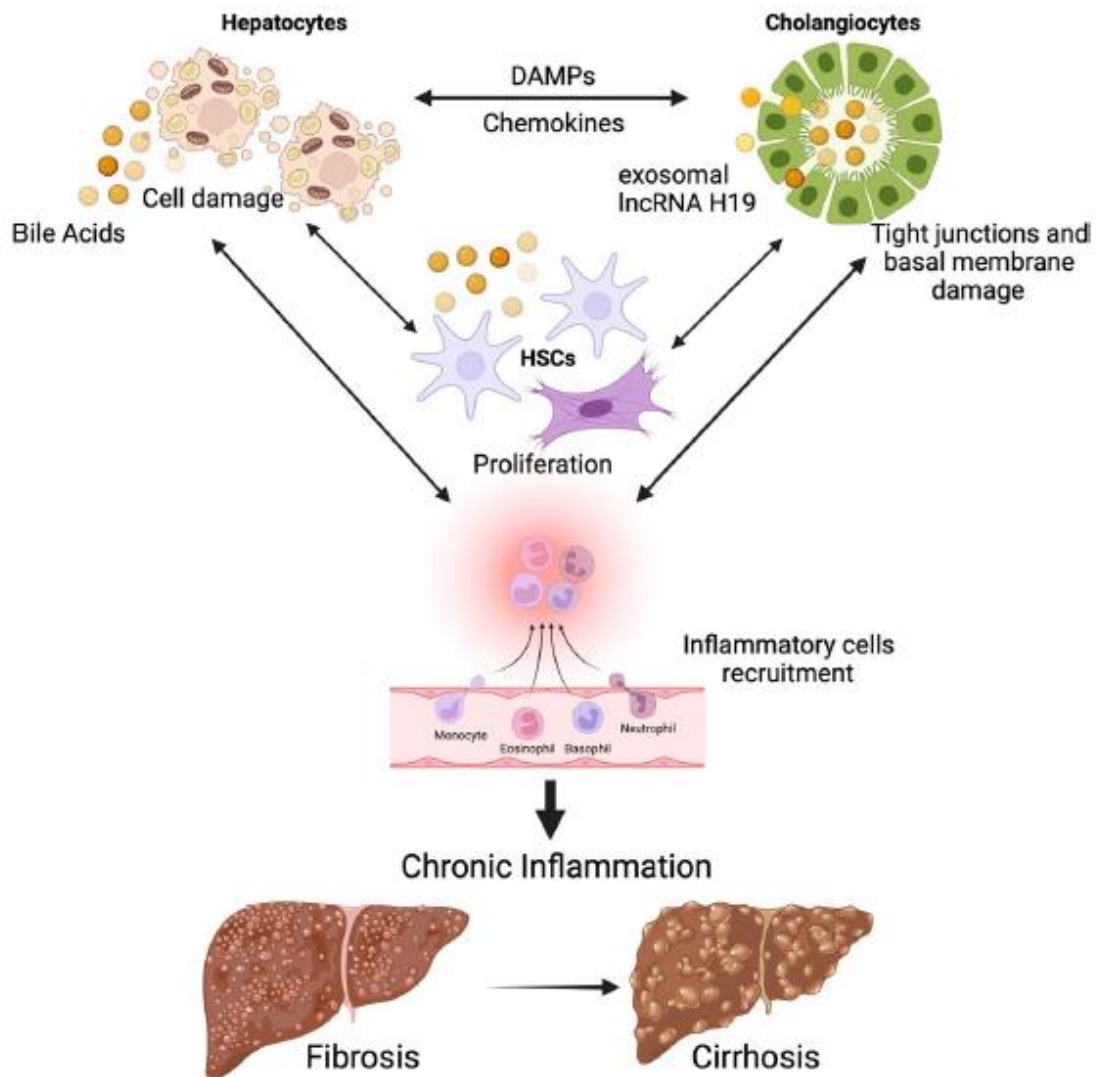


Figure 3. Overview of fibrogenesis in cholestatic liver disease. Various signaling pathways in different cell types are involved in cholestatic liver fibrosis. Damaged hepatocytes secrete chemokines and damage-associated molecular pattern molecules (DAMPs) to activate cholangiocytes, HSCs and inflammatory cells. Bile acid accumulation damages tight junctions and basal membrane of bile ducts, resulting in cholangiocyte activation, inflammation and HSC proliferation and activation. Lasting chronic liver injury eventually leads to cirrhosis. (Taken from Anna Bertolini et al. ³³)

1.3.2 Role of bile salt-induced activation of hepatic stellate cells in fibrogenesis

Activated hepatic stellate cells (HSCs) represent the main source of extracellular matrix deposition characterizing liver fibrosis. Their activation in CLD has been attributed, in part, to pro-fibrotic signals such as transforming growth factor beta (TGF β), apoptotic bodies or DNA derived from damaged hepatocytes²⁶⁻²⁹. While these mechanisms might elegantly explain fibrogenesis in CLD, respective data were hardly been independently reproduced, and *in vivo* evidence for their contribution to liver fibrosis in CLD remains scarce.

Direct activating, pro-fibrogenic effects of bile salts on HSCs have been suggested in the past^{34,35}. We, too, have recently described a direct effect of CDC, the predominating bile salt accumulating in cholestatic liver disease, to induce expansion and extracellular matrix deposition of human and murine HSCs^{30,36}. We could subsequently show that bile salt-induced activation of HSCs was associated with activation of Erk/MEK pathway and partly mediated by the phosphoinositide 3-kinases catalytic subunit p110 α ^{30,37}. These results were in line with previous reports of bile salt-induced activation of pro-proliferatory signaling pathways in HSCs.

In our previous study, only unconjugated CDC but not glycol-conjugated CDC (GCDC), directly induced proliferation and collagen deposition by HSCs^{30,37}. This may give important hints towards the mechanism of HSCs activation by bile salts. While sodium taurocholate co-transporting polypeptide (NTCP) is the major bile salt-uptake transport in hepatocytes³⁸, it is hardly expressed in dormant HSCs³⁹ and its physiologic role in HSCs bile salt homeostasis has been questioned⁴⁰. Given its high hydrophobicity, CDC can passively cross cell

membranes and enter living cells. As previously shown for cholangiocytes, passive entry of bile salts depends on conjugation and the resulting pKa value of bile acid as well as extracellular pH^{41,42}. Additionally, HSCs reside in a microenvironment of slightly acidic pH⁴³ (Figure 4), indicating that bile salts (passive) entry into HSCs may be modulated by extracellular pH (pHe).

The cholestatic mouse model of the bile salt export pump (BESP)-knockout showed that bile salt accumulation failed to induce liver fibrosis in mice³¹. The distinct role of bile salt accumulation in human and murine might be attributed to their different composition of bile salt pool. In humans, chenodeoxycholate (CDC) takes majority and in murine, beta-muricholate (β -MCA) is the biggest part¹⁹. We demonstrated the presence of glycol-conjugated CDC (GCDC) is crucial for development of liver fibrosis in a *in vivo* model of hepatocellular cholestasis³⁰, suggesting that humanized bile salt pool presents more pro-fibrotic than murine bile salt pool in the development of cholestatic liver fibrosis.

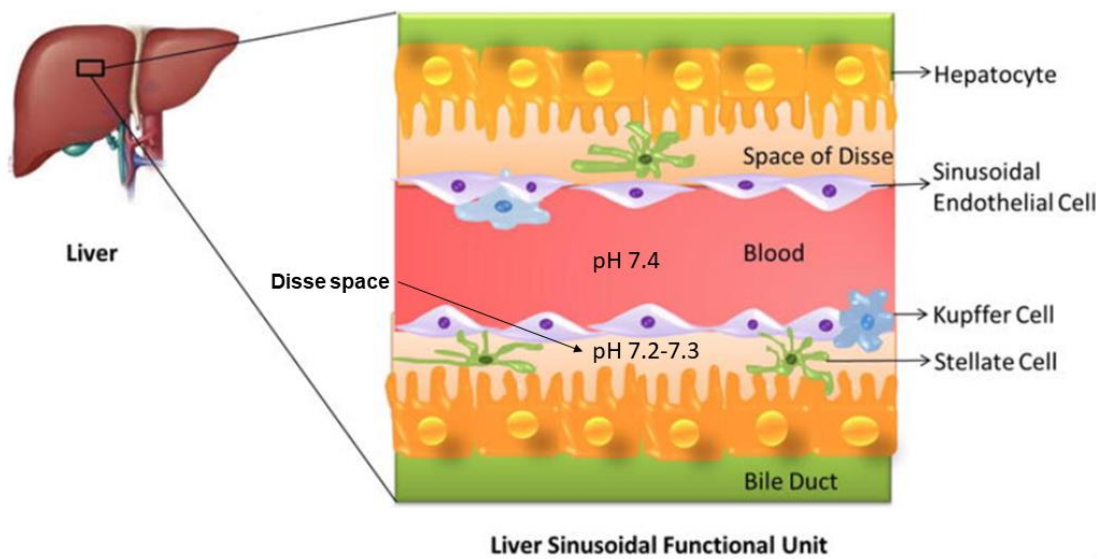


Figure 4. The liver sinusoidal unit.

The liver sinusoid is a capillary formed by sinusoidal endothelial cells separating an additional space from the portal blood stream within the liver. Hepatic stellate cells, together with e.g. Kupffer cells, reside in this “space of Disse”. This compartment has a slightly more acidic pH compared to the main blood stream ⁴³. (modified from Kang YB et al.⁴⁴)

2. Aims

In this project, to further elucidate mechanism of bile salt-induced fibrogenesis and provide new therapeutic strategy, we aim to investigate details as follow:

- 1) Explore the role of humanized bile salt pool in the development of liver fibrosis
- 2) Explore the effect of pHe to bile salt-induced HSC activation
- 3) Explore the therapeutic effect of pHi modulation to cholestatic liver fibrosis

3. Material and methods

3.1 Cell culture

Human HSC line (LX2) was cultured in Dulbecco's Modified Eagle Medium (DMEM) (Sigma-Aldrich, Taufkirchen, Germany) containing 2% fetal bovine serum (FBS, PAN-Biotech, Aidenbach, Germany) and 1% antibiotics (Sigma-Aldrich, Germany) as described previously^{37,45-48}. This standard culture medium for LX2 cells, applied in a standard CO₂ atmosphere of 5% was found to result in a pH of 7.6. Cell medium at pH of 7.6-7.2 were made by proportionately mixing regular DMEM and DMEM without sodium bicarbonate. Cells were cultivated in a humidified atmosphere with 5% CO₂ and 21% O₂ at 37°C. LX2 cells were stimulated with TGF-β (Peprotech, Germany), CDC (Sigma-Aldrich, Taufkirchen, Germany), GCDC (Sigma-Aldrich, Darmstadt, Germany), pantoprazole (PPZ), amiloride (Sigma Aldrich, Italy), bafilomycin A1 (Bafil A1, CST, Germany), sulfasalazine (Sigma-Aldrich, Germany), myrcludex B (Sigma-Aldrich, Germany). LX2 were stimulated with GCDC (100 μM), CDC (20 μM), PPZ (5 μM, 20 μM, 80 μM), amiloride (10 μM, 100 μM), bafilomycin A1 (1nM, 10nM), sulfasalazine (10 μM) and myrcludex B (50 nM).

3.2 Viability assay

1.0×10⁴ to 2.0×10⁴ cells were seeded in 96-well plates for overnight incubation. Stimulation of LX2 with GCDC (100 μM), CDC (20 μM), PPZ (5 μM, 20 μM, 80 μM), amiloride (10 μM, 100 μM) and Bafil A1 (1nM, 10nM), for 24 h. Next, add 10 μl Cell proliferation Reagent WST-1 assay (Roche, Mannheim, Germany) to each well and incu-

bate cells for 2 h. Shake thoroughly for 1 min on a shaker. The absorbance of cells was measured at 450 nm and 690 nm wavelength with the EASY READER SFplus (SLT-Labinstruments, Salzburg, Austria).

3.3 pHi measurement in LX2

The pHi of LX2 was measured by using the cell-permeable probe 3'-O-acetyl-2',7'-bis(carboxyethyl)-5,6-carboxyfluoresceinacetoxymethyl ester (BCECF-AM). 1.0×10^4 to 2.0×10^4 cells were cultured in a 96-well plate at 37 °C for overnight incubation, and then co-treatment of LX2 with GCDC (100 μ M), CDC (20 μ M), PPZ (5 μ M, 20 μ M, 80 μ M), amiloride (10 μ M, 100 μ M) and Bafil A1 (1nM, 10nM) for 24 h. After that, cells were incubated with BCECF-AM for 30 min at 37 °C in full humidity with 5% CO₂. Cells were washed twice with the HEPES buffer, and 100 μ L/well of HEPES buffer. pH calibration was made by high K⁺ solutions (140 mM) at different pH values (7.8, 7.4, 7.0, 6.6, 6.0), buffered with HEPES or MOPS and 10 μ M Nigericin (Invitrogen, USA). The fluorescence intensity was determined using a fluorescent plate reader with an excitation wavelength of 450nm/490nm, and 535 nm emission wavelength (PerSeptive Biosystems, Framingham, MA, USA).

3.4 Measurement of bile salt accumulation in LX2

The bile salt accumulation in LX2 was evaluated by fluorometric quantification of Cholyl-Lysyl-Fluorescein (CLF), a bile salt analogue. 1.0×10^4 to 2.0×10^4 cells were cultured in a 96-well plate at 37 °C for overnight incubation, and then co-treatment of LX2 with PPZ (5 μ M, 20 μ M, 80 μ M), amiloride (10 μ M, 100 μ M), Bafil A1 (1nM, 10nM), sulfasalazine (10 μ M) and myrcludex B (50 nM) for 24 h. Next, cells

were incubated with CLF (5 μ M) at 37 °C for 30 min and washed twice with HBSS. Fluorescence was measured with 100 μ L/well of HEPES buffer in a plate reader (Cyto Fluor 4000 PerSeptive Biosystems, Framingham, MA, USA) at wavelength of excitation 485 nm and emission 530 nm.

3.5 DNA quantification assay

6,000-7,000 cells were cultured in a 96-well plate at 37 °C for overnight incubation, and then co-treatment of LX2 with GCDC (100 μ M), CDC (20 μ M), PPZ (5 μ M, 20 μ M, 80 μ M), amiloride (10 μ M, 100 μ M) and Bafil A1 (1nM, 10nM) for 24 h.

- (1) Removed medium and added 100 μ l 0.1% SDS to each well and froze cells in -18°C overnight.
- (2) Prepared 10 \times TE solution: 1 ml 20 \times TE + 9 ml sterile water
- (3) Made Picogreen assay by 1:200 of Picogreen:10 \times TE
- (4) Added 100 μ l Picogreen assay into 96-well plate which contains 0.1% SDS and shake for half hour.
- (5) The total DNA amount in cells as a surrogate of cell number was determined by the PicoGreen[®] dsDNA assay (Invitrogen, Carlsbad, USA) with a CytoFluor Multi-Well Plate Reader Series 4000 (PerSeptive Biosystems, Framingham, MA, USA).

3.6 Reverse-transcription quantitative polymerase chain reaction (RT-qPCR)

mRNA gene expression of ACTA2, TGF β 1, PDGFB, LOX, COL1 α 1, TMIP1 and β -ACTIN were measured by RT-qPCR. Total RNA from mouse liver tissue was isolated with TranszolUp reagent (TransGen Biotech, China). Total purified RNA was amplified by PerfectStart Green qPCR SuperMix (TransGen Biotech, China) and translated into

cDNA by EasyScript[®] One-Step gDNA Removal and cDNA synthesis SuperMix (TransGen Biotech, China). Quantitative PCR was performed with CFX Connect[™] Real-Time System (Bio-Rad, USA). All qPCR primers used are listed in Table 1. mRNA Expression was calculated according to $\Delta\Delta CT$ method with β -actin as the house-keeping gene and normalized to the means of the controls.

Table 1. Primers Information for Reverse-Transcription Quantitative Polymerase Chain Reaction Gene name.

	Forward	Reverse
ACTA2	G TTCAGTGGTGCCTCTGTCA	ACTGGGACGACATGGAAAAG
TGF β 1	CTTCAATACGTCAGACATTCCGGG	GTAACGCCAGGAATTGTTGCTA
PDGFB	AAGTGTGAGACAATAGTGACCCC	CATGGGTGTGCTTAAACTTTTCG
LOX	GACCCCTACTACATCCAGGC	AAGTCCGATGTCCCTTGGTT
Col1 α 1	TAAGGGTCCCCAATGGTGAGA	GGGTCCCTCGACTCCTACAT
TMIP1	ACCACCTTATACCAGCGTTATGA	GGTGTAGACGAACCGGATGTC
IL1 β	TGCCACCTTTTGACAGTGATG	AAGGTCCACGGGAAAGACAC
β -actin	G TTCAGTGGTGCCTCTGTCA	ACTGGGACGACATGGAAAAG

3.7 Western blotting

Proteins were loaded in equal amounts, separated by 10% SDS-PAGE for 1 h at 150 V and transferred onto PVDF membrane (Merck-Millipore, Darmstadt, Germany). Membranes were blocked in 1% casein (Carl Roth, Karlsruhe, Germany) for 30 min and incubated with primary antibodies against α -smooth muscle actin (α SMA, CST, Germany), collagen type I alpha I (col1 α 1, Abcam, USA) and GAPDH (Sigma-Aldrich, Darmstadt, Germany) overnight at 4 °C followed by incubation with secondary goat anti-mouse IgG-HRP (Bio-Rad, Feld-

kirchen, Germany). Visualization was performed with Clarity™ Western ECL Substrate (Bio-Rad, Feldkirchen, Germany), detected with the ChemoCam (INTAS, Göttingen, Germany)

3.8 Na⁺/H⁺ activity measurement

Na⁺/H⁺ activity was determined as reported earlier⁴⁹ by studying pHi change upon removal and re-introduction of extracellular Na⁺: LX2 suspension was seeded with 24*24 mm glass cover slides in φ35 mm petri dish. Cells were divided into control and PPZ (2.5, 5, 10, 20, 40, 80 μM) treatment groups when the cell confluency reached 60%-80%. After 4 h PPZ treatment, cells were washed twice with Na⁺-Hepes buffer. Cells were incubated at 37 °C for 30 min in 1 mL Na⁺-Hepes containing 5 μM BCECF-AM. Cells were washed again twice with Na⁺-Hepes buffer. Glass slides were placed on the microscope stage of Ratio Photometry and Imaging Systems (PTI, USA) and continuously perfused with Na⁺-free HEPES-buffered solutions by gravity (0-3 min: Na⁺-free HEPES buffer; 3-8 min: Na⁺-containing HEPES buffer with 10 μM Nigericin; 8-11 min: Na⁺-free HEPES buffer with 1% BSA; 11-14 min: Na⁺-free HEPES-buffer; 14-20 min: Na⁺-containing HEPES buffer). BCECF-AM module of PTI was applied to measure pHi of cells with Na⁺-free HEPES buffer. The fluorescent dye was excited at 440 and 485 nm alternatively and recorded every 30 s. pHi alteration of cells during 14-17 min was calculated to represent Na⁺/H⁺ exchanger activity.

3.9 Animals

All animal protocols were conducted following the animal welfare act and Bavarian state regulations for animal experiment. Male C57BL/6J mice (8 weeks of age) were maintained at 22°C with a 12-hour:12-

hour light/dark cycle and had free access to normal chow diet and water.

Carbon tetrachloride (CCl₄)-GCDC model: Mice were randomly allocated into four groups: control diet, GCDC (0.1% w/w) diet, control diet + CCl₄, GCDC (0.1% w/w) diet + CCl₄. Mice were fed a control diet or a diet enriched GCDC (0.1% w/w) for 6 weeks to humanize their bile salt pool. For the last 4 weeks, mice were treated with CCl₄ (0.93 g/kg) 3 times per week. Mice were sacrificed after 6 weeks. Liver tissue and plasma were collected.

Bile duct ligation (BDL)-GCDC model: Mice were randomly allocated into four groups: control diet, GCDC (0.1% w/w) diet, control diet + BDL, GCDC (0.1% w/w) diet + BDL. Mice were fed a control diet or a diet enriched GCDC (0.1% w/w) for 4 weeks to humanize their bile salt pool. at the beginning of the third week, mice were treated with BDL surgery. Mice were sacrificed after 4 weeks. Liver tissue and plasma were collected. These experiments (permitted to use) have been conducted at the Department of Gastroenterology, Affiliated hospital of Zunyi Medical University, China.

BDL-PPZ model: Mice were randomly allocated into three groups: the sham, BDL-sterile H₂O, BDL-PPZ. The BDL protocol was performed as previously described⁵⁰. 1 day after surgery, BDL mice were injected i.p. by sterile H₂O and 5 mg/Kg PPZ dissolved in sterile H₂O twice per day for 14 d. Mice were sacrificed after 14 d. Liver tissue and plasma were collected. These experiments (permitted to use) have been conducted at the Department of Gastroenterology, Affiliated hospital of Zunyi Medical University, China.

3,5-Diethoxycarbonyl-1,4-Dihydrocollidine (DDC)-PPZ model: Mice were randomly allocated into three groups: the control, 0.01% DDC-

sterile H₂O, DDC-PPZ. Mice were fed a control diet or a diet enriched 0.01% DDC. DDC-diet mice were injected i.p. by sterile H₂O and 5 mg/Kg PPZ dissolved in sterile H₂O twice per day for 4 weeks. Mice were sacrificed after 4 weeks. Liver tissue and plasma were collected. These experiments (permitted to use) have been conducted at the Department of Gastroenterology, Affiliated hospital of Zunyi Medical University, China.

3.10 Bile acid analysis

Concentrations of bile acids in serum were measured by LC-MS/MS. The levels of total bile acids were the sum of all bile acids quantified in samples. Tauro- ω -muricholate (T ω MC), Tauro- α -muricholate (T α MC), Tauro- β -muricholate (T β MC), taurocholate (TC), taurodeoxycholate (TDC), taurochenodeoxycholate (TCDC), glycocholate (GC), glycodeoxycholate (GDC), GCDC were measured to determine humanized or murine bile salt pool.

3.11 Serum analysis

Serum aspartate aminotransferase (AST), alanine aminotransferase (ALT) and total bilirubin (TBIL) were measured by Beckman AU5800 Chemistry Analyzer using kits purchased from Beckman Coulter Inc. (USA). Liver samples were fixed with 4% formaldehyde.

3.12 Liver histology

Liver samples were fixed with 4% formaldehyde. After embedding in paraffin, 3 μ M sections were stained with hematoxylin and eosin (H&E) for liver damage measurement, Sirius red and Masson staining for liver fibrosis measurement, according to standard protocols.

H&E:

- (1) Dewax and dehydration
- (2) Staining: Hematoxylin for 5 min → water wash for 5 min → hydrochloric acid alcohol for 2-3 s → water wash for 10 min → 0.5% Eosin for 1 min → water wash for 5 min.
- (3) Dehydration

Sirius red:

- (1) Dewax and dehydration
- (2) Prepare Sirius red staining solution at 2:1 of Sirius red solution and Greenfixation solution. Staining for 60 min and then water wash for 5 min.
- (3) Dehydration

Masson trichrome:

- (1) Dewax and dehydration
- (2) Masson dye solution for 5 min → water wash for 5 min → phosphomolybdic acid for 5 min → dry slides → aniline blue for 5 min → water wash for 5 min
- (3) Dehydration

3.13 Immunohistochemistry

Paraffin-embedded sections (3 μ M) of liver tissues were used for immunohistochemical staining. Anti- α -SMA polyclonal rabbit antibody (Abcam UK) were applied as primary antibody. HRP-labeled polymer anti-rabbit antibody (Boster, China) was applied as second antibody. The specific staining was visualized by light microscopy.

3.14 Statistical analysis

All in vitro experiments were repeated more than three times. For all animal experiments, 5 or more than 5 samples were included in each group. Statistical calculations were performed by using SPSS 25 (IBM, USA) or GraphPad Prism 7 (USA) using analysis of t-Test, analysis of variance (ANOVA) with appropriate post-hoc tests (Fisher's least significant difference (LSD) or Tukey's). P-values lower than 0.05 were referred to as statistically significant. All data are presented as mean \pm standard deviation.

4. Results

4.1 GCDC feeding induces a humanized bile salt pool in BDL and CCl₄ mouse models

A humanized bile salt pool by GCDC feeding independently induced liver fibrosis in a model of hepatocellular cholestasis³⁰. To further explore the role of humanized bile salt pool in the development of liver fibrosis, mouse models of general liver fibrosis (CCl₄) and extrahepatic cholestasis (BDL) were analyzed. A humanized bile salt pool was induced by feeding a GCDC-enriched diet vs. control. While GCDC was hardly detected in healthy mice with control diet, GCDC feeding led to a rise in GCDC plasma level (1.1%) (Figure 5A). GCDC plasma level increased from 0.03% in BDL mice with control diet to 22.9% in BDL mice with GCDC supplementation (Figure 5A). For other human major bile salts, GCDC feeding led to a rise in GC and GDC from 0.4% and 0.01% to 2.7% and 0.2% in BDL mice, respectively. Furthermore, GCDC feeding decreased murine major bile salts, including T ω MC, T β MC, TC and TDC from 5.4%, 8.9%, 10.3% and 40.6% to 0.3%, 2.5%, 0.03% and 15.8% in healthy mice, and from 1.4%, 46.6%, 12.6% and 0.2% to 0.4%, 32.1%, 9.1% and 0.1% in BDL mice (Figure 5A), respectively. Importantly, results showed no significant increases in total bile salts level between control diet mice and GCDC-enriched diet mice, with or without BDL (Figure 5B). In total, these results indicate that GCDC feeding led to a shift of bile salt composition towards a humanized bile salt pool, without increasing total bile salt concentrations. In the CCl₄ mouse model, we also noticed a shift towards a humanized bile salt pool with CDC-derivates, including CDC, GCDC and TCDC, increasing from 1.2%, 0%, and 1.4 to 6.7%, 0.6% and 5.4% with GCDC feeding

(Figure 6A), respectively. However, in this setting, GCDC feeding also increased total levels of bile salts compared to mice with control diet, with or without CCl₄ injection (Figure 6B).

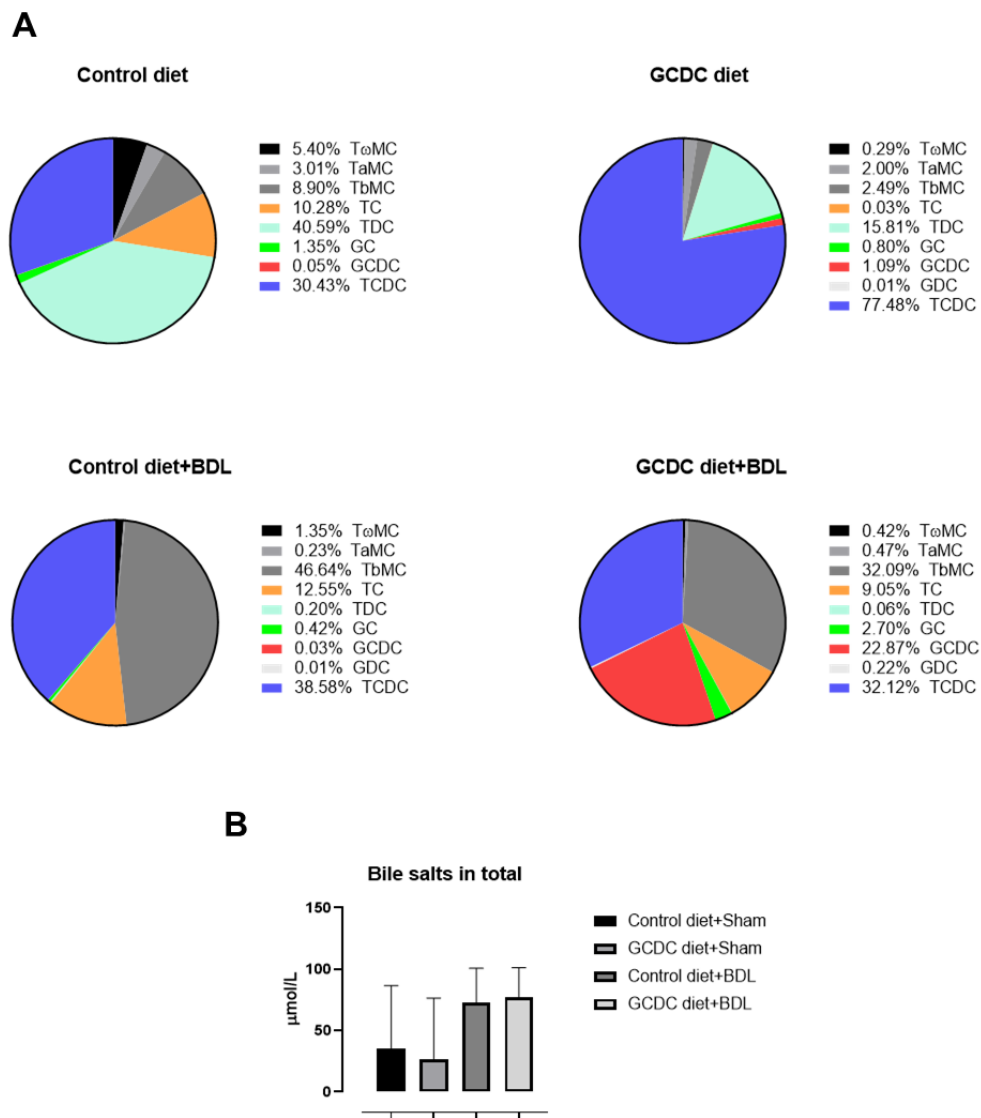


Figure 5. GCDC feeding humanized the bile salt pool in the mouse model of BDL.

C57BL/6 male mice aged 4-6 weeks were fed with control or GCDC diet (0.1% w/w) for 4 weeks and were performed with or without BDL at the beginning of 3rd week. Bile salt compositions (A) and bile salts total concentrations were determined (B). (n=5-10; *, p <0.05; **, p <0.01, compared to control; #, p <0.05; ##, p <0.01, compared to positive model; t-test, ANOVA, post-hoc LSD or Tukey)

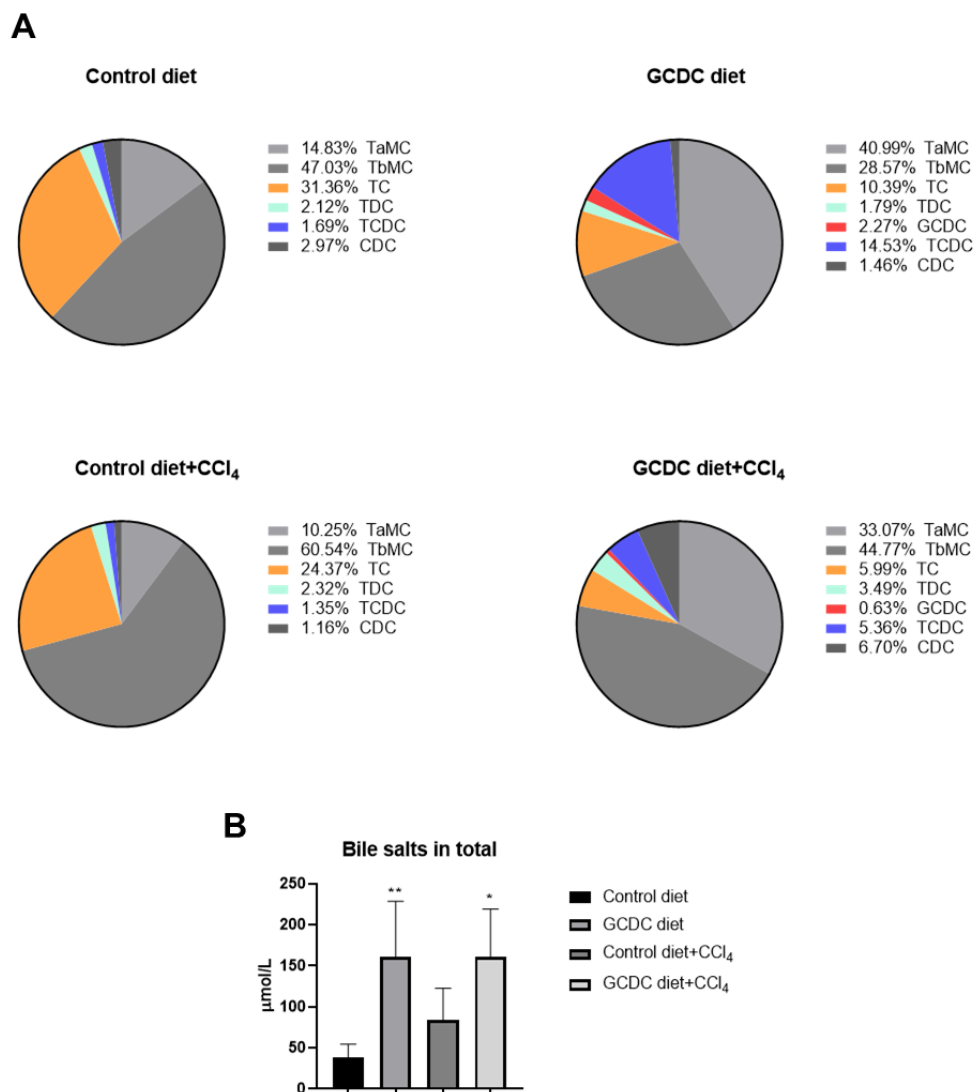


Figure 6. GCDC feeding humanized the bile salt pool in the mouse model of CCl₄.

C57BL/6 male mice aged 4-6 weeks were fed with control or GCDC diet (0.1% w/w) for 6 weeks and were administered with or without CCl₄ (0.93 g/kg), 3 times a day, i.p., for the last 4 weeks. Bile salt compositions (A) and bile salts total concentrations were determined (B). (n=5-10; *, p <0.05; **, p <0.01, compared to control; #, p <0.05; ##, p <0.01, compared to positive model; t-test, ANOVA, post-hoc LSD or Tukey)

4.2 Humanized bile salt pool aggravates liver fibrosis in mouse models of CLD

To explore the impact of bile salt composition on liver fibrosis in mice, Masson staining and Sirius red staining were performed, quantifying collagen deposition. In both models, GCDC feeding showed no promotion for liver fibrosis development in control animals (i.e., no-BDL, no-CCl₄ controls).

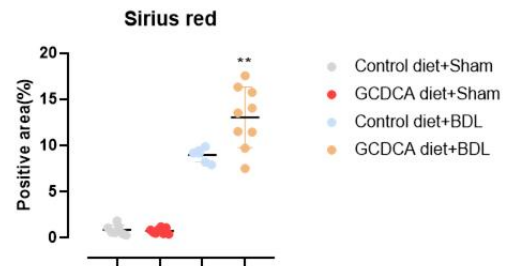
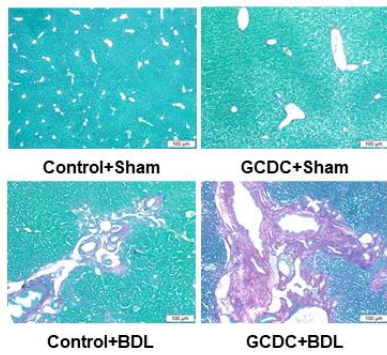
Following BDL, GCDC supplementation significantly aggravated liver fibrosis as evidenced by Masson and Sirius red staining (Figure 7A-B). This observation was confirmed by immunohistochemistry for α SMA expression (Figure 7C). In serum biochemistry, AST and ALT as markers for liver damage as well as total bilirubin as a marker of advanced liver disease showed no changes between control diet mice and GCDC-enriched diet mice, with or without BDL (Figure 7D-F).

In CCl₄ treated mice, too, GCDC supplementation significantly aggravated liver fibrosis as evidenced by Sirius red staining and liver hydroxyproline measurement (Figure 8A-B). This observation was confirmed further by Western blotting for α SMA expression (Figure 8E). In serum biochemistry, ALT as markers for liver damage as well as total bilirubin as a marker of advanced liver disease showed no changes between control diet mice and GCDC-enriched diet mice, with or without CCl₄ (Figure 8C and D).

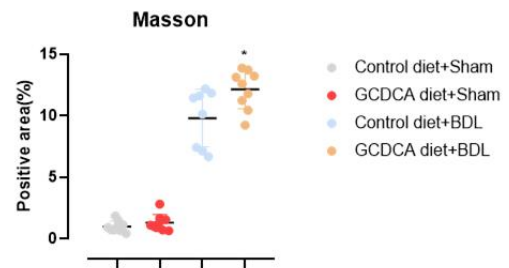
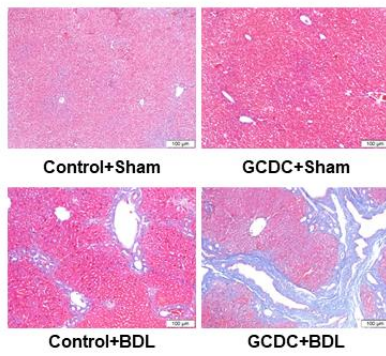
Collectively, GCDC feeding alone, in otherwise control-treated animals, did not lead to liver damage. Even when BDL or CCl₄ treatment were introduced, no effect on gross liver damage (ALT, AST) could be observed. Liver fibrosis following BDL and CCl₄, however, was specifically promoted and more advanced in the presence of a humanized bile salt pool.

In summary, humanization of the bile salt pool following GCDC feeding not only promotes liver fibrosis development in models of cholestasis, but also in causes of liver fibrosis.

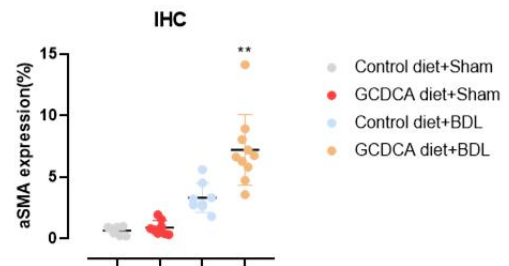
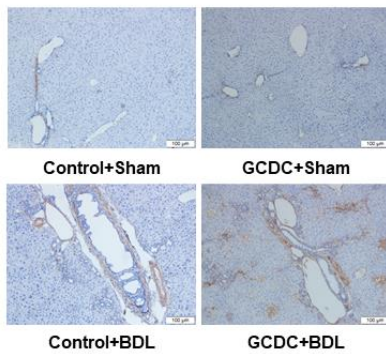
A



B



C



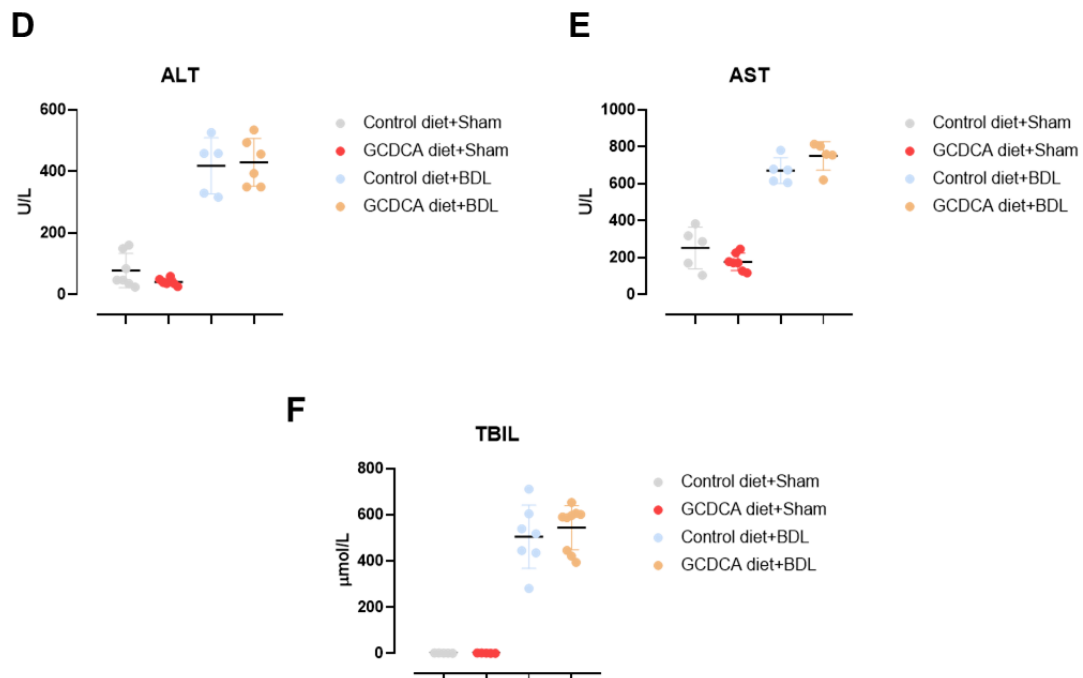


Figure 7. GCDCA feeding-induced human-like bile salt pool aggravated liver fibrosis in a BDL mouse model.

C57BL/6 male mice aged 4-6 weeks were fed with control or GCDCA diet (0.1% w/w) for 4 weeks and were performed with or without BDL at the beginning of 3rd week. Representative images for H&E, Masson staining, Sirius red staining and IHC for α SMA are given in (A-C). Quantitative assessment (% of total area) is given for Masson staining (A), Sirius red staining (B) and IHC for α SMA (C) is presented. From serum biochemistry, levels of ALT (D), AST (E) and total bilirubin (F) are given. (n=5-10; *, p <0.05; **, p <0.01, compared to control; #, p <0.05; ##, p <0.01, compared to positive model; t-test, ANOVA, post-hoc LSD or Tukey)

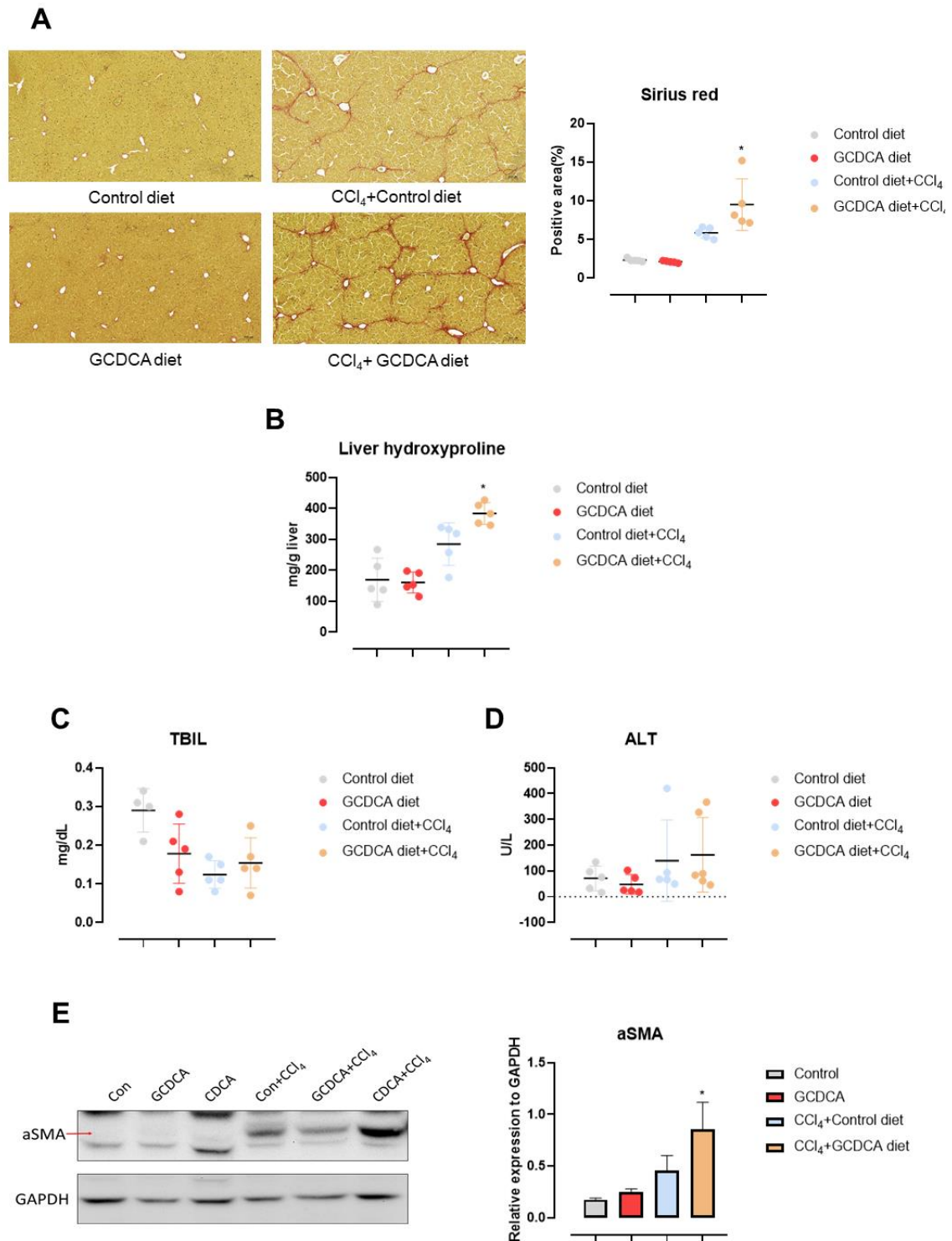


Figure 8. GDCD feeding-induced human-like bile salt pool aggravated liver fibrosis in a CCl₄ mouse model.

C57BL/6 male mice aged 4-6 weeks were fed with control or GDCD diet (0.1% w/w) for 6 weeks and were administered with or without CCl₄ (0.93 g/kg), 3 times a day, i.p., for the last 4 weeks. Representative images for Sirius red staining are

given in (A). Quantitative assessment (% of total area) is given for Sirius red staining (A) is presented. Liver hydroxyproline is determined (B). From serum biochemistry, levels of total bilirubin (C) and ALT (D) are given. α SMA protein expression was determined by Western Blotting and representative images for α SMA protein are shown as well as quantitative analysis of α SMA normalized for GAPDH (E). (n=5-10; *, p <0.05; **, p <0.01, compared to control; #, p <0.05; ##, p <0.01, compared to positive model; t-test, ANOVA, post-hoc LSD or Tukey)

4.3 CDC, but not GCDC, induces activation of HSC in standard cell culture conditions

We have previously shown that presence of GCDC, the predominant hydrophobic bile salt accumulating in chronic cholestatic liver disease in humans, is a prerequisite for the development of liver fibrosis in models of hepatocellular cholestasis³⁰. As discussed above, various (indirect) mechanisms have been proposed to explain fibrogenesis in cholestasis, such as the release of apoptotic bodies from dying hepatocytes. Here, we tested the ability of (G)CDC to directly activate HSCs *in vitro*. While CDC in low micromolar concentrations (20 – 50 μ M), expectedly, induced α SMA expression in LX2 (Figure 9A), GCDC was unable to activate LX2 cells when applied in standard culture medium in concentrations up to 500 μ M (Figure 9B). In light of the considerable cytotoxicity of GCDC at concentrations from 250 μ M (Figure 9C), we did not test stimulatory effects of higher doses. CDC, at the stimulatory concentrations applied, did not induce relevant cytotoxicity (Figure 9D). Bile salt uptake, i.e., intracellular accumulation, was tested by use of the bile salt analogue cholyl-lysyl-fluorescein (CLF). We found that CLF after stimulation for 1 hour accumulated in LX2 and intracellular fluorescence was dose dependent (Figure 9E).

In brief, GCDC, unlike CDC, was unable to activate HSC at standard cell culture conditions. A hypothetical explanation for this difference is the lower pKa of GCDC compared to CDC, which comes with a higher protonation rate and thus polarity of the molecule, with reduced ability for passive cell entry.

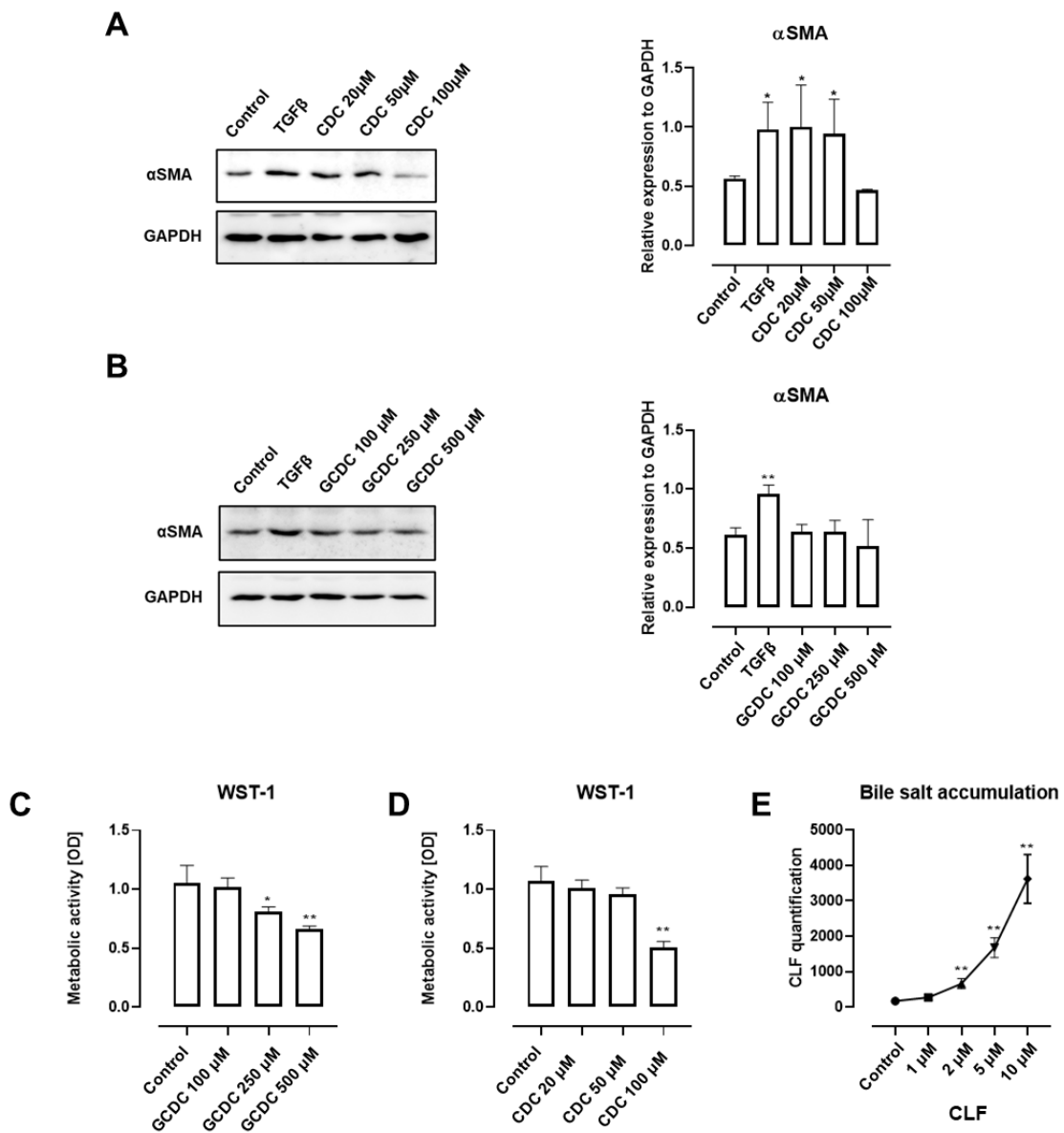


Figure 9. GCDC, unlike CDC, is unable to activate LX2 cells in standard culture conditions.

LX2 cells were stimulated with CDC (A) or GCDC (B) for 24 hours at the concentrations indicated and α SMA expression was quantified by western blotting in relation to GAPDH. TGF β was used as a positive control. (C, D) Cell viability was

assessed using WST-1 assays after 24 hours of stimulation. (E) LX2 cells were incubated with CLF at pH 7.3 for 1 hour at the indicated concentrations and intracellular fluorescence was quantified. (n=4-5; * p <0.05, ** p <0.01, compared to control; # p <0.05, ## p <0.01, compared to (G)CDC groups; t-test, ANOVA, post-hoc LSD or Tukey)

4.4 Activation of HSC by (G)CDC is crucially determined by extracellular pH

In consequence of its lower pKa, GCDC compared to CDC requires a more acidic pH for protonation. This would, theoretically, enable an increase in passive cell entry. Considering the slightly acidic pH (pH 7.2 – 7.3) in the space of Disse, where dormant HSCs reside, this might be physiologically relevant⁴³. To test this hypothesis, we took a closer look at cell culture medium pH as part of the cellular micro-environment.

Standard culture conditions for LX2 cells have repeatedly been reported as follows: DMEM containing 2% FBS, cultivated in a humidified atmosphere with 5% CO₂ and 21% O₂ at 37°C^{37,45-48}. After allowing this standard culture medium (cell free) to adjust in the CO₂ atmosphere for 24 hours, pH was measured and a pH of 7.64 ± 0.1 (n=5) was found. Adjusting the bicarbonate buffer system in the cell culture medium, pH-controlled medium of pH 7.6, 7.5, 7.4, 7.3 and 7.2 was applied for subsequent experiments. While pH modification was overall well-tolerated, cell viability started to decline from pH 7.2 (Figure 10D).

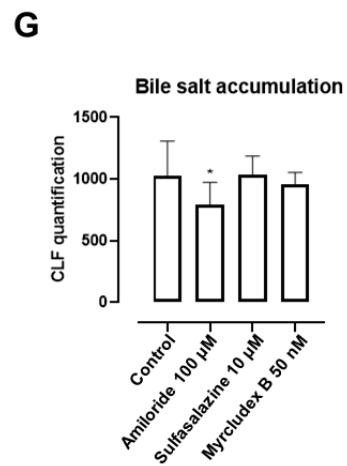
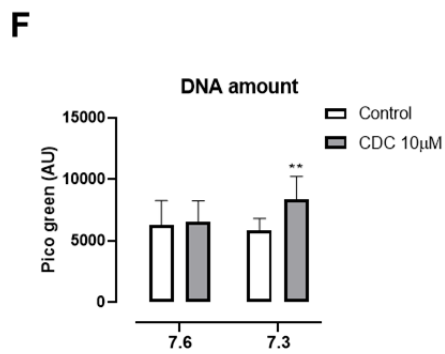
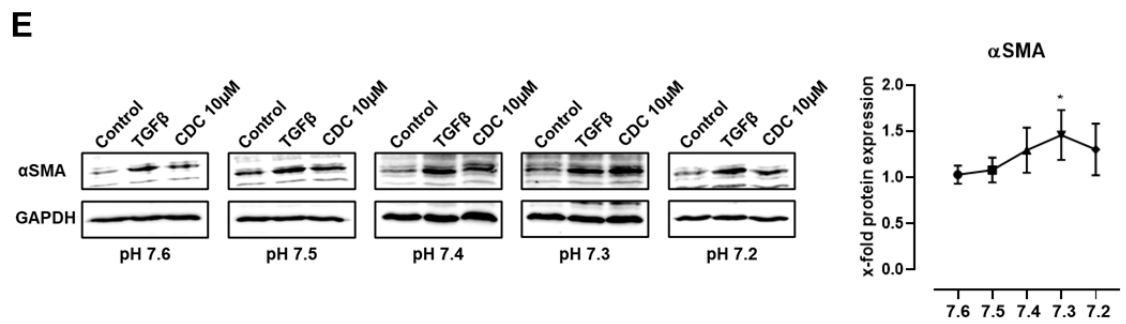
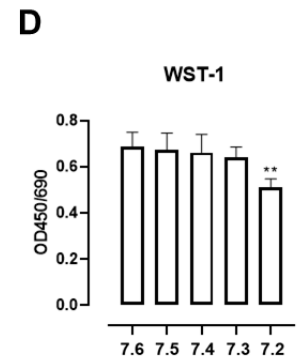
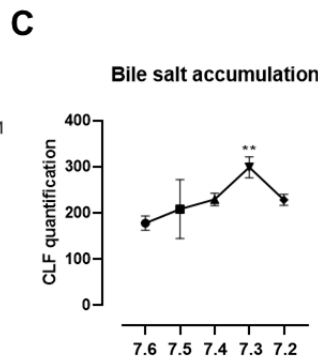
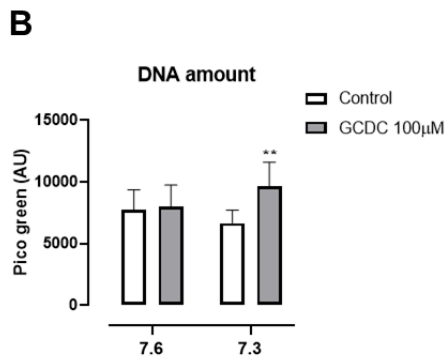
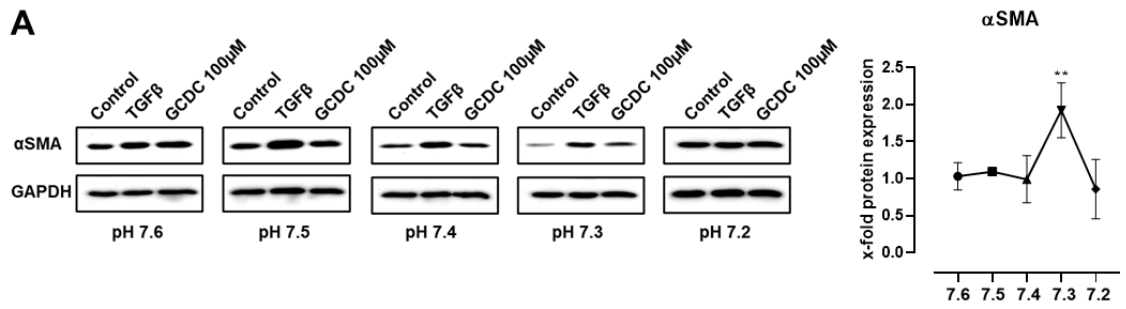
While GCDC (100 µM) was unable to activate LX2 in a standard culture condition, a 1.9±0.4-fold protein expression of αSMA was induced at pH 7.3 (n=4, p<0.01, ANOVA, Tukey) (Figure 10A).

Picogreen assay was performed to quantify DNA amount as a surrogate for cell proliferation. We found GCDC at 100 μM to induce LX2 proliferation at pHe 7.3, while no stimulation was documented at pH 7.6 (Figure 10B). According to our hypothesis, increased activation of LX2 by GCDC at lower pH would be a result of increased bile salt uptake or accumulation. To assess whether bile salt uptake in LX2 is indeed influenced by pHe, we fluorometrically quantified intracellular accumulation of the bile salt analogue CLF. As predicted, CLF accumulation increased with stepwise reduction of pHe from 7.6 to 7.3 (Figure 10C). If the increase in bile salt-induced activation of LX2 at lower pH was a general principle based on a pH-dependent increase in bile salt uptake, the same effect should be detectable for CDC. We therefore applied a lower dose of CDC (10 μM), which had earlier been found to be unable to activate LX2 cells at standard culture conditions, and tested its ability to activate LX2 at various pHe conditions. As seen for GCDC, cells were increasingly activated with lowering pHe. αSMA expression was increased 1.1 ± 0.1 , 1.3 ± 0.2 and 1.5 ± 0.3 -fold at pH 7.5, 7.4 and 7.3, respectively, compared to control (Figure 10E). CDC-induced cell proliferation, too, was dependent on pHe in LX2 cells (Figure 10F).

The role of active bile salt uptake via specific transporters in HSC is under debate^{39,40}. To exclude transporter-mediated uptake in our system, inhibitors of NTCP and organic anion transporting polypeptide (OATP) were applied, myrcludex B and sulfasalazine, respectively^{51,52}. We found that both inhibitors, sulfasalazine and myrcludex B, neither altered bile salt, i.e., CLF accumulation nor CDC- or GCDC-induced activation for LX2 (Figure 10G-I).

Taken together, these results suggest that extracellular pH, known to be slightly acidic in the natural microenvironment of HSCs, crucially

determines (passive) bile salt uptake and (G)CDC-induced activation and proliferation of HSC.



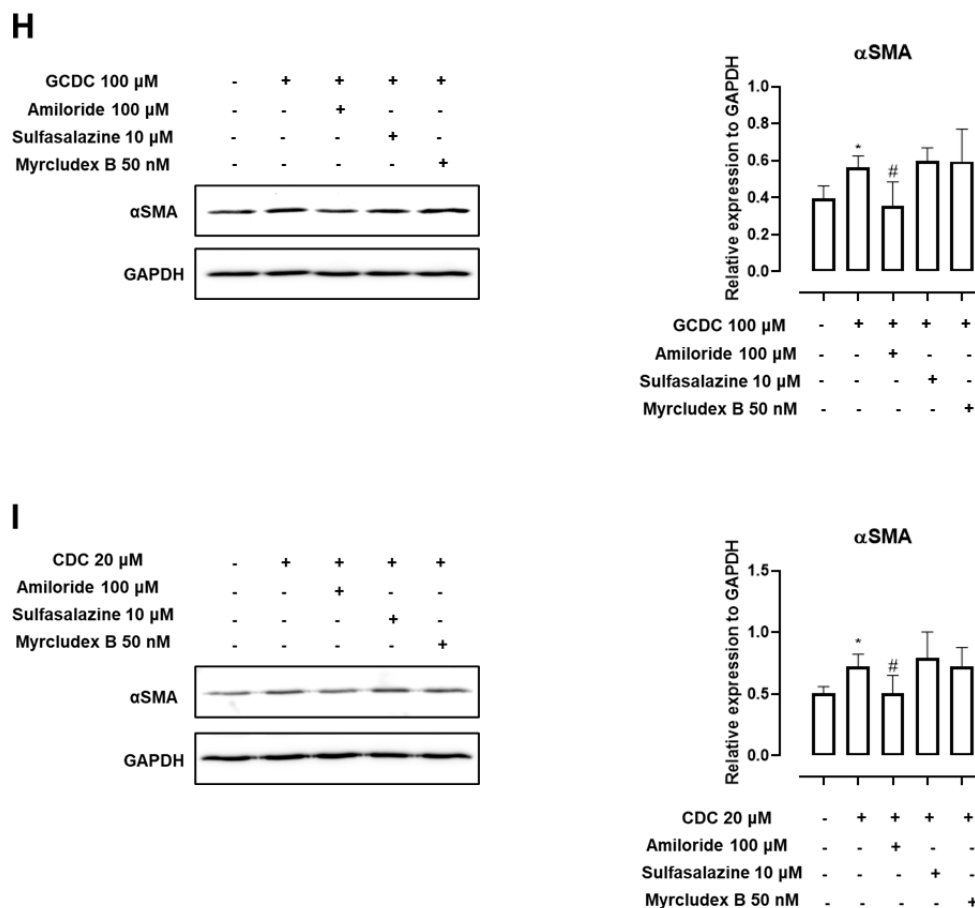


Figure 10. Extracellular pH determines intracellular bile salt accumulation and bile salt-induced activation of LX2 cells.

LX2 cells were stimulated with GCDC (100 μ M) for 24h in buffered culture medium to test various pHe values (7.6 – 7.2). Subsequently, α SMA protein expression was determined by Western Blotting and representative images for α SMA protein are shown as well as quantitative analysis of α SMA normalized for GAPDH (A). Furthermore, DNA amount as a surrogate of proliferation was quantified by Picogreen assays (B). LX2 cells were incubated in presence of CLF at various pHe (7.6 – 7.2) for 1 hour and accumulation was determined fluorometrically (C). Cell viability was assessed using WST-1 assays after 24 hours of stimulation (D). LX2 cells were stimulated with CDC (10 μ M) for 24h in buffered culture medium to test various pHe values (7.6 – 7.2). Subsequently, α SMA protein expression was determined by Western Blotting and representative images for α SMA protein are shown as well as quantitative analysis of α SMA normalized for GAPDH (E). Furthermore, DNA amount as a surrogate of proliferation was quantified by Picogreen assays (F). After 24 hours stimulation with sulfasalazine (10

μM) and myrcludex B (50 nM), LX2 were incubated with CLF for 1 hour to determine bile salt accumulation. Amiloride was used as positive control, as will become evident in Figure 5 (G). αSMA protein expression was determined by Western Blotting and representative images are shown as well as quantitative analysis of αSMA , normalized for GAPDH (H-I). (n=4-5; * $p < 0.05$, ** $p < 0.01$, compared to control; # $p < 0.05$, ## $p < 0.01$, compared to (G)CDC groups; t-test, ANOVA, post-hoc LSD or Tukey)

4.5 Inhibition of sodium-hydrogen exchanger in HSC leads to intracellular acidification, prevents bile salt uptake and (G)CDC-induced HSC activation

While extracellular pH cannot be pharmacologically addressed, the transcellular pH gradient can be targeted by alteration of intracellular pH. This might offer a pharmacological target to prevent pro-fibrogenic signaling of bile salts. PPZ, the most widely used proton pump inhibitor is known for inactivating H^+/K^+ -ATPase in the gastric mucosa but may also target alternative proton pumps. In HSC, NHE has previously been implicated in pHi regulation⁵³⁻⁵⁵. We measured NHE activity in LX2 cells, and found it to be dose-dependently reduced following incubation with PPZ (Figure 11A). Subsequently, we determined pHi in LX2 following incubation with PPZ and again found a dose-dependent decrease (5 μM – 80 μM) (Figure 11B). Next, to assess whether PPZ can affect bile salt accumulation, CLF was used and was observed to accumulate less as LX2 were pre-treated with PPZ for 24 hours (Figure 11C). To determine whether PPZ can alter pHi in LX2 also in the presence of bile salts, LX2 were simultaneously stimulated with PPZ and GDC for 24 hours. Following incubation with GDC, LX2 cells were found to have a higher pHi compared to

control treated cells (Figure 11D). This was in line with previous reports showing that activated HSCs had higher pHi in comparison to dormant HSCs⁵³. Of note, also in presence of GCDC, PPZ reduced pHi in a dose-dependent manner (Figure 11D). Decreased pHi and bile salt uptake in presence of PPZ was associated with an amelioration of GCDC-induced activation of LX2 cells as indicated by a reduction in α SMA and collagen type I alpha I (col1 α 1) expression (Figure 11E). Furthermore, proliferation induced by GCDC was prevented by PPZ in a dose-dependent manner, as suggested by Picogreen assays (Figure 11F). Importantly, WST-1 assays did not show evidence of cell toxicity exerted by PPZ plus GCDC (Figure 11G). All effects of PPZ on pHi, LX2 activation and proliferation could be reproduced when CDC (20 μ M) was applied instead of GCDC (Figure 12A-D).

In summary, we could show that inhibition of intracellular proton pumps, i.e., the NHE in LX2 cells leads to a decrease in pHi, prevents bile salt uptake and is associated with an inhibition of bile salt-induced HSC activation.

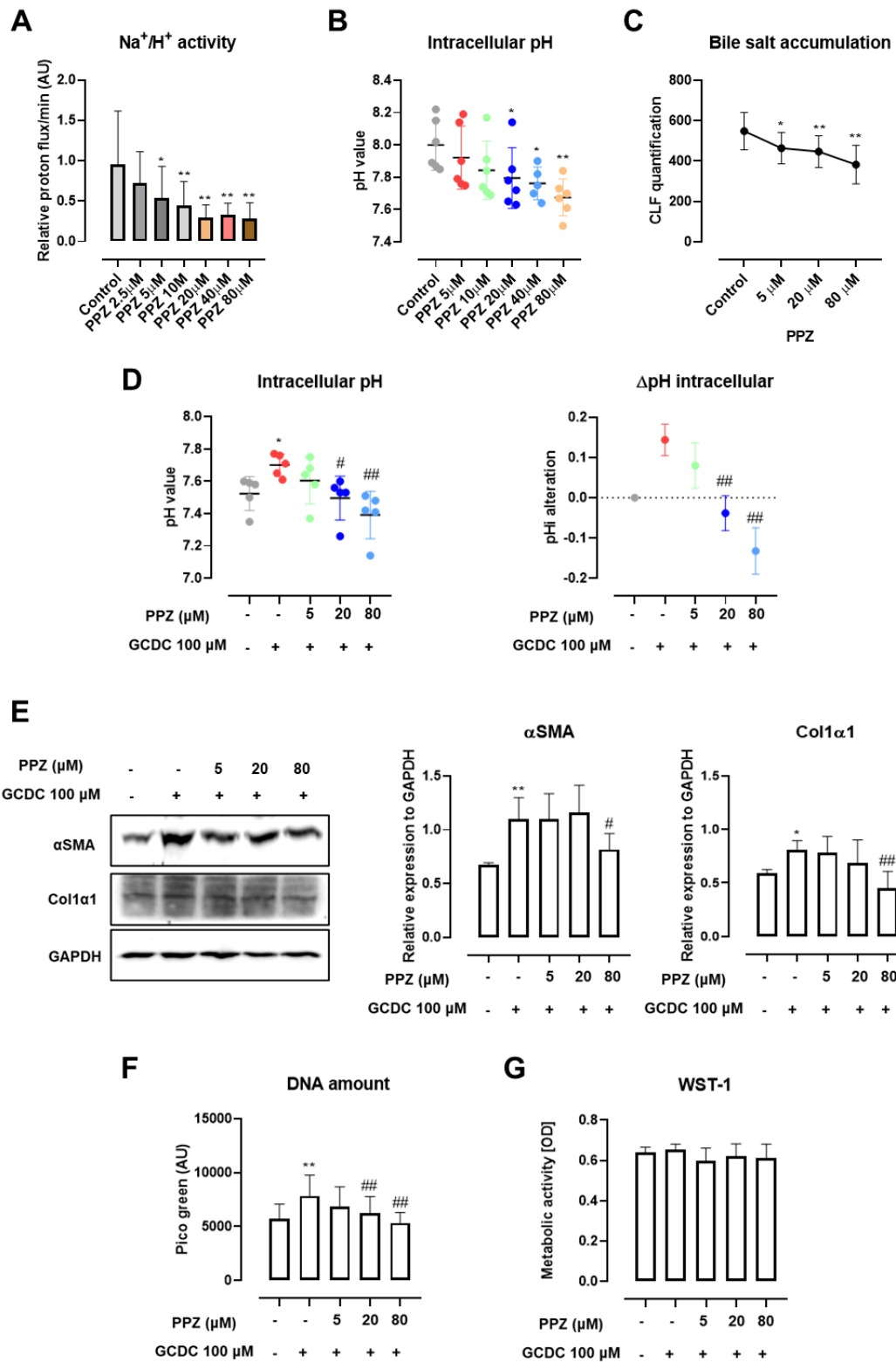


Figure 11. PPZ inhibits Na⁺/H⁺ exchanger to lower pHi and is associated with protection against bile salt entry and GCDC-induced pro-fibrogenic activation in LX2.

LX2 cells were pre-treated with PPZ (2.5-80 μM) for 24 h in buffered culture medium at pH 7.3. Subsequently, Na^+/H^+ activity (A), pHi (B), and bile salt accumulation (C) were determined. Furthermore, LX2 cells were simultaneously stimulated with GDC (100 μM) and PPZ (5-80 μM) for 24 h in buffered culture medium at pH 7.3. Subsequently, pHi was determined (D), as well as αSMA and $\text{col1}\alpha 1$ protein expression (E, representative blot and densitometric analysis), DNA amount as a surrogate of proliferation (F) and cell viability, quantified by WST-1 assays (G). (n=4-6; * p <0.05, ** p <0.01, compared to control; # p <0.05, ## p <0.01, compared to (G)CDC groups; t-test, ANOVA, post-hoc LSD or Tukey)

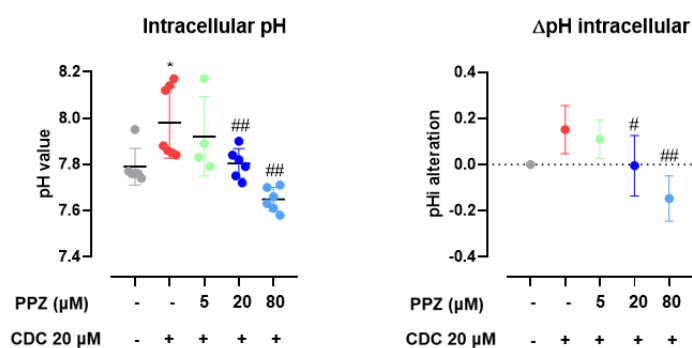
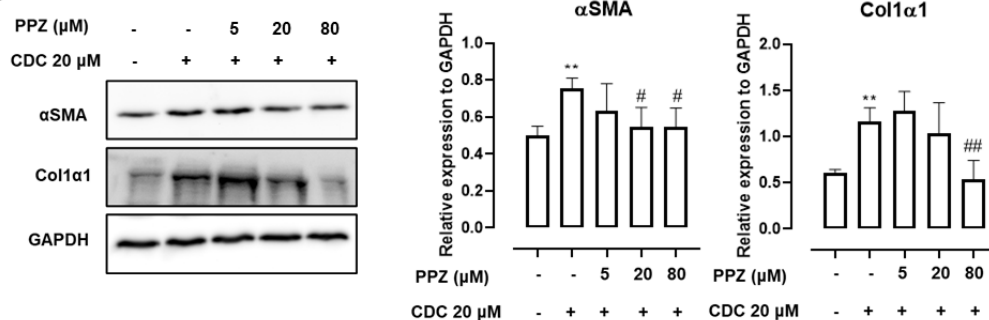
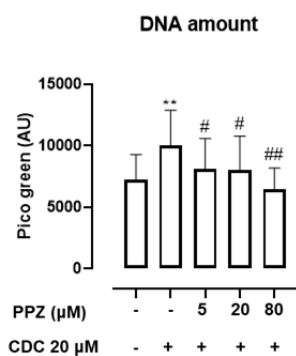
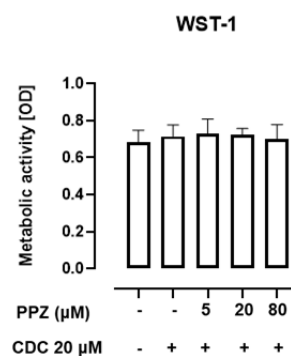
A**B****C****D**

Figure 12. CDC-induced activation of LX2 is ameliorated by PPZ, associated with pHi alteration

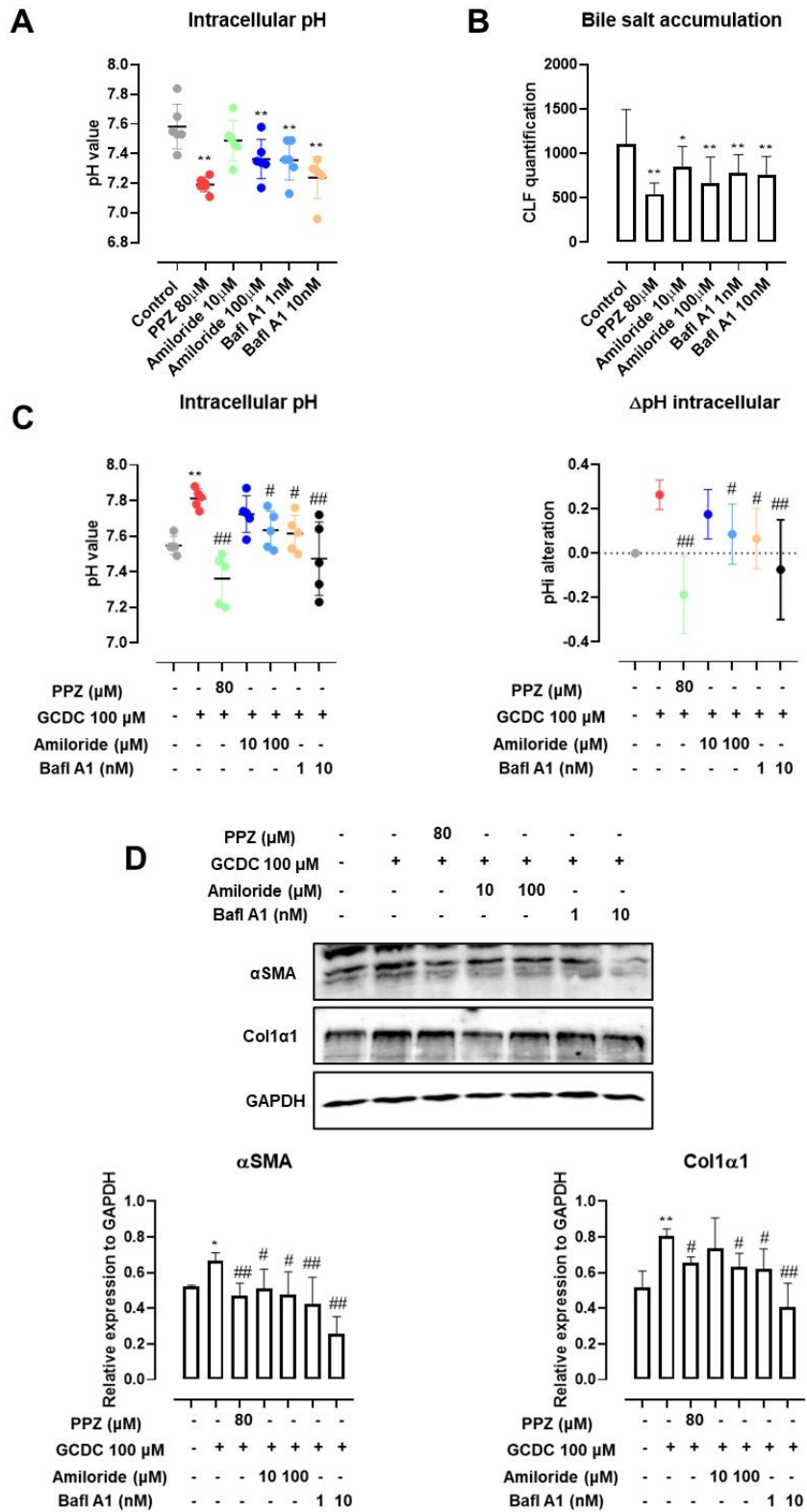
LX2 cells were simultaneously stimulated with CDC (20 μ M) and PPZ (5-80 μ M) for 24 h in buffered culture medium at pHe 7.3. Subsequently, pHi was determined (A). α SMA and col1 α 1 protein expression was determined by Western Blotting and representative images are shown as well as quantitative analysis of α SMA and col1 α 1, normalized for GAPDH (B). Furthermore, DNA amount as a surrogate of proliferation was quantified by Picogreen assays (C). Cell viability was quantified by WST-1 assays (D). (n=4-5; * p <0.05, ** p <0.01, compared to control; # p <0.05, ## p <0.01, compared to (G)CDC groups; t-test, ANOVA, post-hoc LSD or Tukey)

4.6 (G)CDC-induced HSCs activation is ameliorated by proton pump inhibitors targeting NHE and vacuolar(v)-H⁺-ATPase

Was the anti-fibrotic effect of PPZ attributable to pHi change or could it be due to pleiotropic effects of PPZ? To further validate a specific, pHi-mediated effect, an additional, established inhibitor of NHE was used, amiloride. Since v-H⁺-ATPase has been established as an additional potent pHi regulator in HSCs⁵⁶, its inhibitor bafilomycin A1 was additionally tested. We found that amiloride (10 μ M, 100 μ M) and bafilomycin A1 (1nM, 10nM) were effective in lowering pHi in LX2 in absence (Figure 13A) and presence (Figure 13B) of GCDC, and inhibited bile salt accumulation in LX2 (Figure 13C). In consequence, both amiloride and bafilomycin A1 ameliorated GCDC-induced activation of LX2 as determined by α SMA and col1 α 1 at protein expression (Figure 13D) as well as proliferation as determined by Picogreen assays (Figure 13E). WST-1 assays showed no toxicity of the inhibitors used in presence of GCDC (Figure 13F). Identical effects were found when CDC was applied instead of GCDC (Figure 14A-D).

To further clarify the role of potential pleiotropic, anti-fibrotic effects of the inhibitors applied, as opposed to specific action via pHi-alteration, the effects of PPZ, amiloride and bafilomycin A1 on TGF β -induced LX2 activation were determined. Bafilomycin A1 ameliorated LX2 activation also in this setting, hinting towards an additional pleiotropic effect. However, we found that amiloride 10-100 μ M did not affect TGF β -induced LX2 activation (Figure 8G), suggesting an anti-fibrotic effect specific to bile salt-induced HSC activation. PPZ ameliorated TGF β -induced activation to some extent, although with lower efficacy compared to that seen in bile salt-induced LX2 activation.

Thus, pHi modification in LX2 by various proton pump inhibitors prevented bile salt-induced HSCs activation and proliferation.



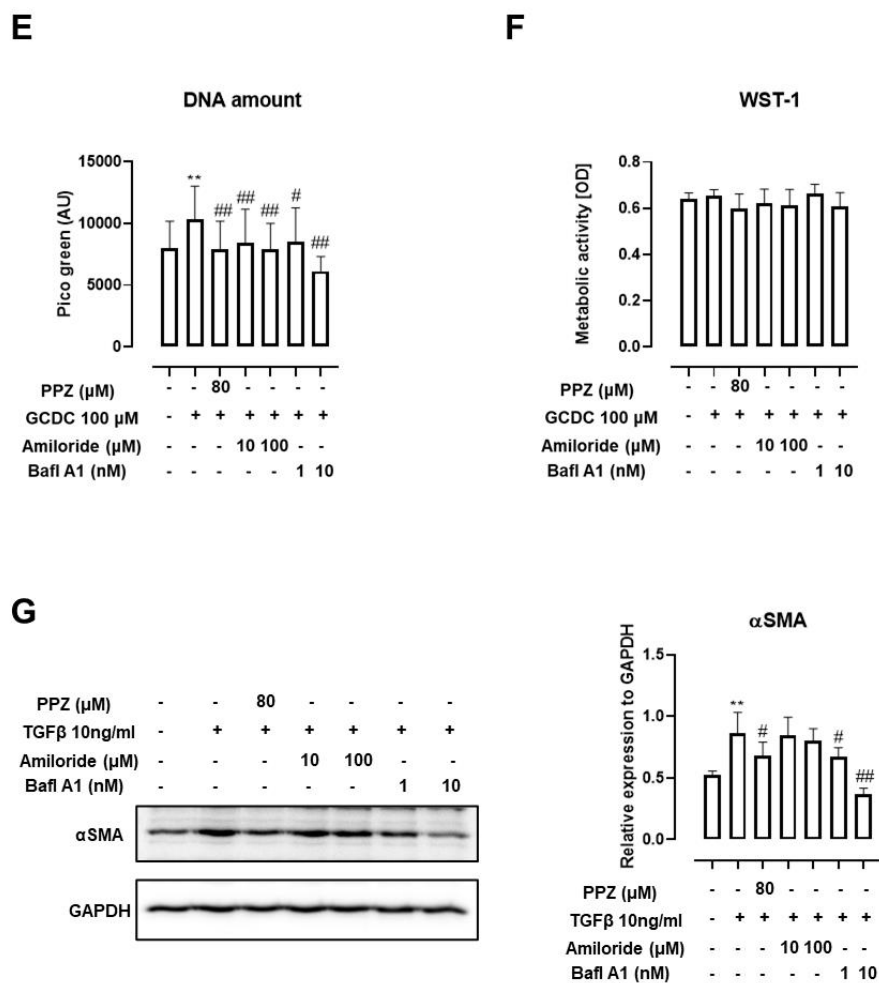


Figure 13. Amiloride and bafilomycin A1 alter pHi and inhibit GCDC-induced activation of LX2.

LX2 cells were stimulated with amiloride (10-100 μM) or bafilomycin A1 (1-10 nM) for 24h in buffered culture medium at pHe 7.3. Based on results from figures 2 and 3, PPZ (80 μM) was used as a positive control for pHi alteration. Subsequently, pHi values (A) and bile salt accumulation (B) were determined. Subsequently, experiments were repeated in presence of GCDC (100 μM) and pHi was determined (C). αSMA and col1α1 protein expression were determined by Western Blotting and representative images are shown as well as quantitative analysis of αSMA and col1α1, normalized for GAPDH (D). Furthermore, DNA amount as a surrogate of proliferation was quantified by Picogreen assays (E). Cell viability was quantified by WST-1 assays (F). In independent experiments, LX2 cells were stimulated with TGFβ (10 ng/ml) for 24 hours in presence or absence of PPZ (80 μM), amiloride (10-100 μM) and bafilomycin A1 (1-10 nM), respectively. αSMA

protein expression was determined by Western Blotting and representative images are shown as well as quantitative analysis of α SMA, normalized for GAPDH (G). (n=4-5; * p <0.05, ** p <0.01, compared to control; # p <0.05, ## p <0.01, compared to (G)CDC groups or TGF β ; t-test, ANOVA, post-hoc LSD or Tukey)

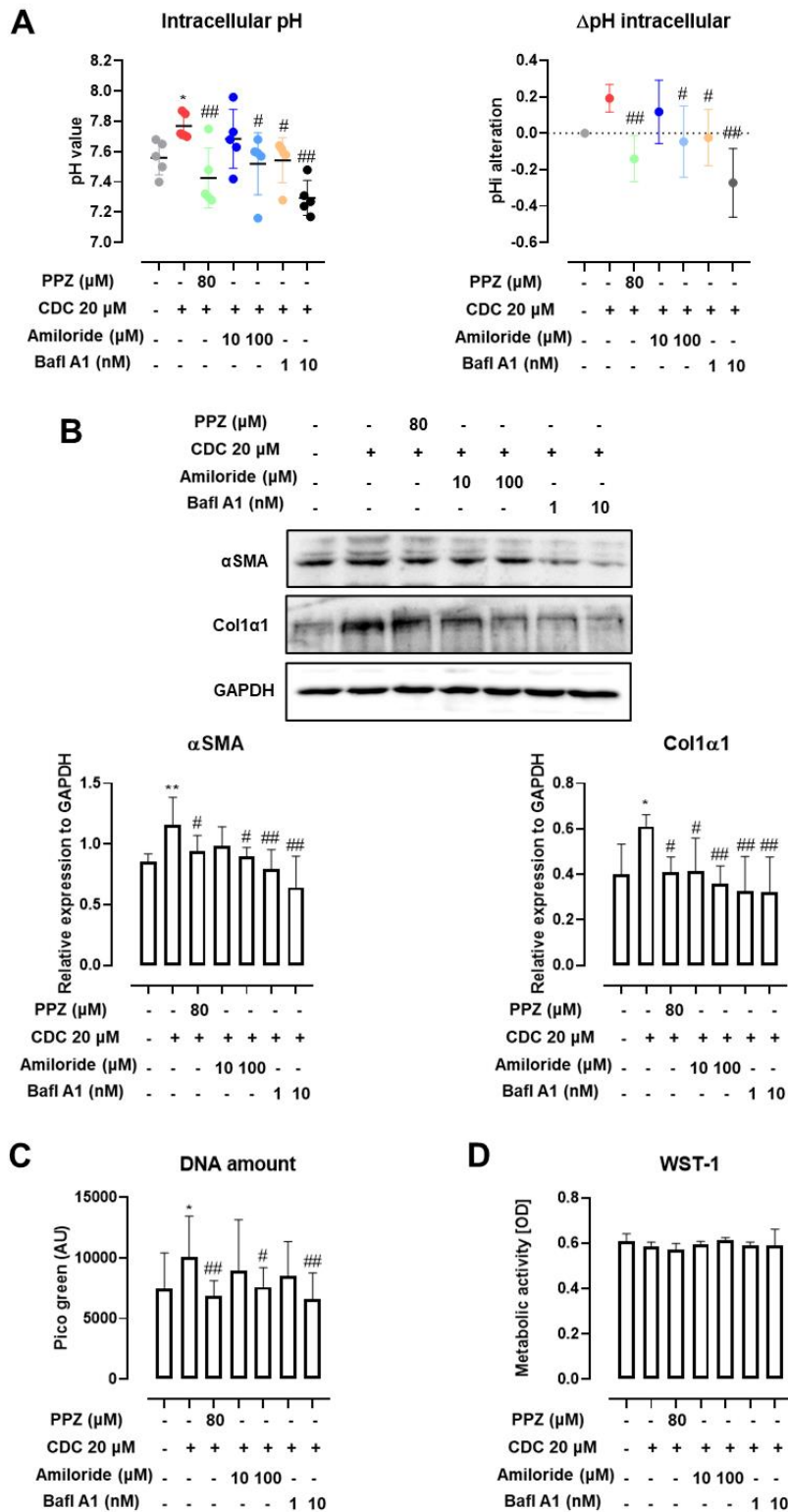


Figure 14. Amiloride and bafilomycin A1 alter pHi and inhibit CDC-induced activation of LX2.

LX2 cells were stimulated with amiloride (10-100 μ M) or bafilomycin A1 (1-10 nM) for 24h in buffered culture medium at pHe 7.3. Experiments were performed in presence of CDC (20 μ M) and pHi was determined (A). α SMA and col1 α 1 protein expression were determined by Western Blotting and representative images are shown as well as quantitative analysis of α SMA and col1 α 1, normalized for GAPDH (B). Furthermore, DNA amount as a surrogate of proliferation was quantified by Picogreen assays (C). Cell viability was quantified by WST-1 assays (D). (n=4-5; * p <0.05, ** p <0.01, compared to control; # p <0.05, ## p <0.01, compared to (G)CDC groups or TGF β ; t-test, ANOVA, post-hoc LSD or Tukey)

4.7 Pantoprazole prevents liver fibrosis in the DDC-diet model of chronic cholestasis

Since proton pump inhibition in HSC prevented bile salt-induced fibrogenesis *in vitro*, we aimed at translating our results into an *in vivo* system. Among available proton pump inhibitors, PPZ is the clinically best established. Therefore, to test its potential to prevent liver fibrosis in cholestasis *in vivo*, PPZ was applied in the DDC-diet model. Evaluation of H&E stains showed minor tissue damage but significant inflammation in DDC-fed mice, which was unaltered upon PPZ administration (Figure 15A and B). Despite a lack in improvement of liver inflammation, Sirius red as well as Masson staining detected a decrease in DDC-induced liver fibrosis following PPZ treatment (Figure 15A, C, D). This was confirmed by immunohistochemistry for α SMA (Figure 15A, E). In serum biochemistry, ALT and AST as markers for liver damage as well as alkaline phosphatase as a marker of cholestasis were markedly increased in DDC-fed mice, as expected. No improvement in these biochemical markers was observed when PPZ

was applied (Figure 15F-H), indicating that the severity of primary liver damage was not altered by PPZ. Total bilirubin, however, representing a serum marker of advanced liver disease, i.e., fibrosis, was slightly but significantly improved upon PPZ administration (Figure 15I). Furthermore, pro-fibrotic markers TIMP1 and PDGFB were significantly downregulated by PPZ on mRNA level (Figure 15J, K).

Taken together, these *in vivo* data suggest that PPZ does not prevent cholestasis, liver damage or liver inflammation in the DDC mouse model of chronic cholestasis, but specifically ameliorates activation of pro-fibrogenic pathways and liver fibrosis.

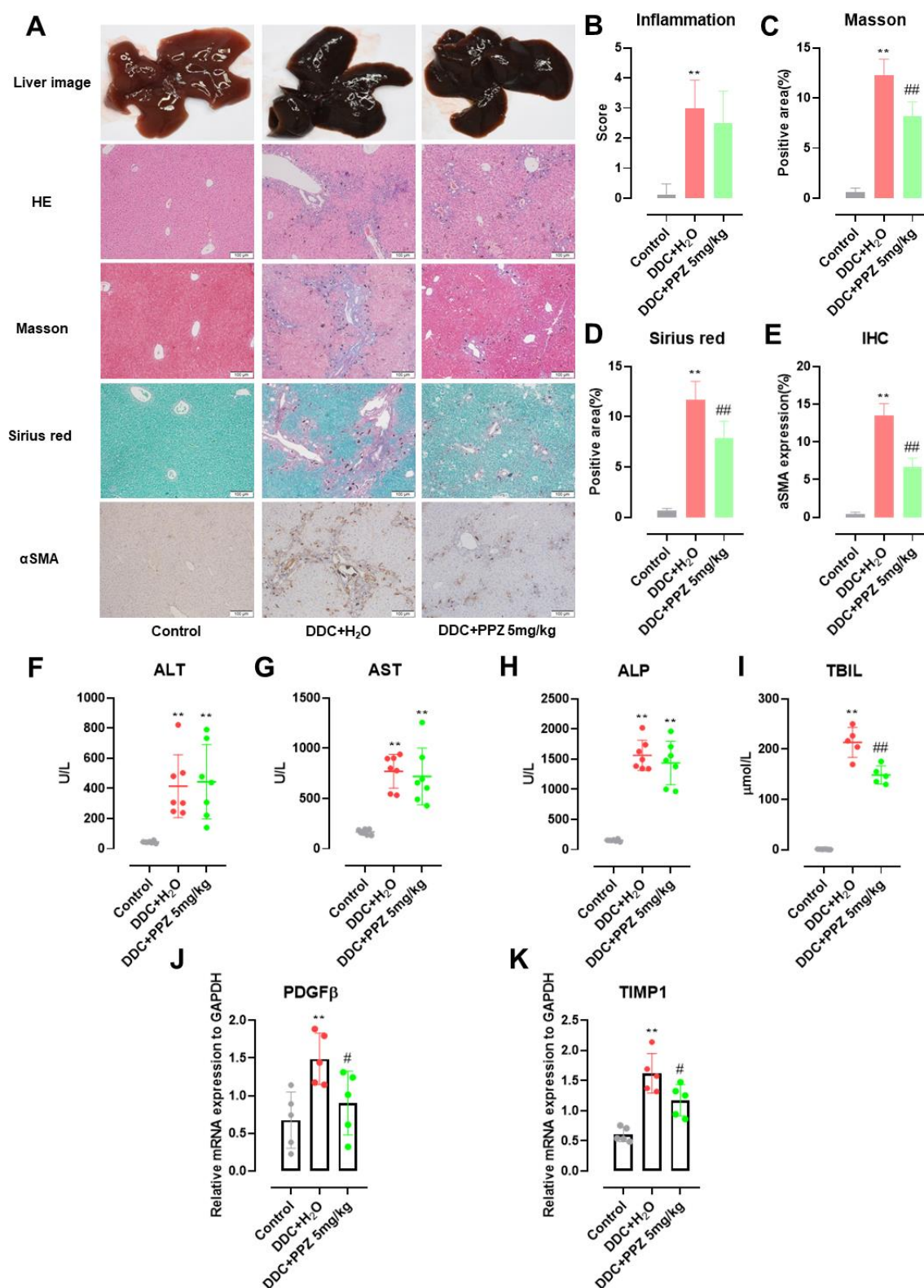


Figure 15. PPZ ameliorates DDC-induced cholestatic liver fibrosis in mice.

C57BL/6 male mice aged 4-6 weeks were fed with control or DDC diet (0.1%) and were administered with H₂O as control or PPZ at 5 mg/kg, twice a day, i.p., for 4 weeks. Representative images for general macroscopic appearance, H&E, Masson staining, Sirius red staining and IHC for αSMA are given in (A). Liver

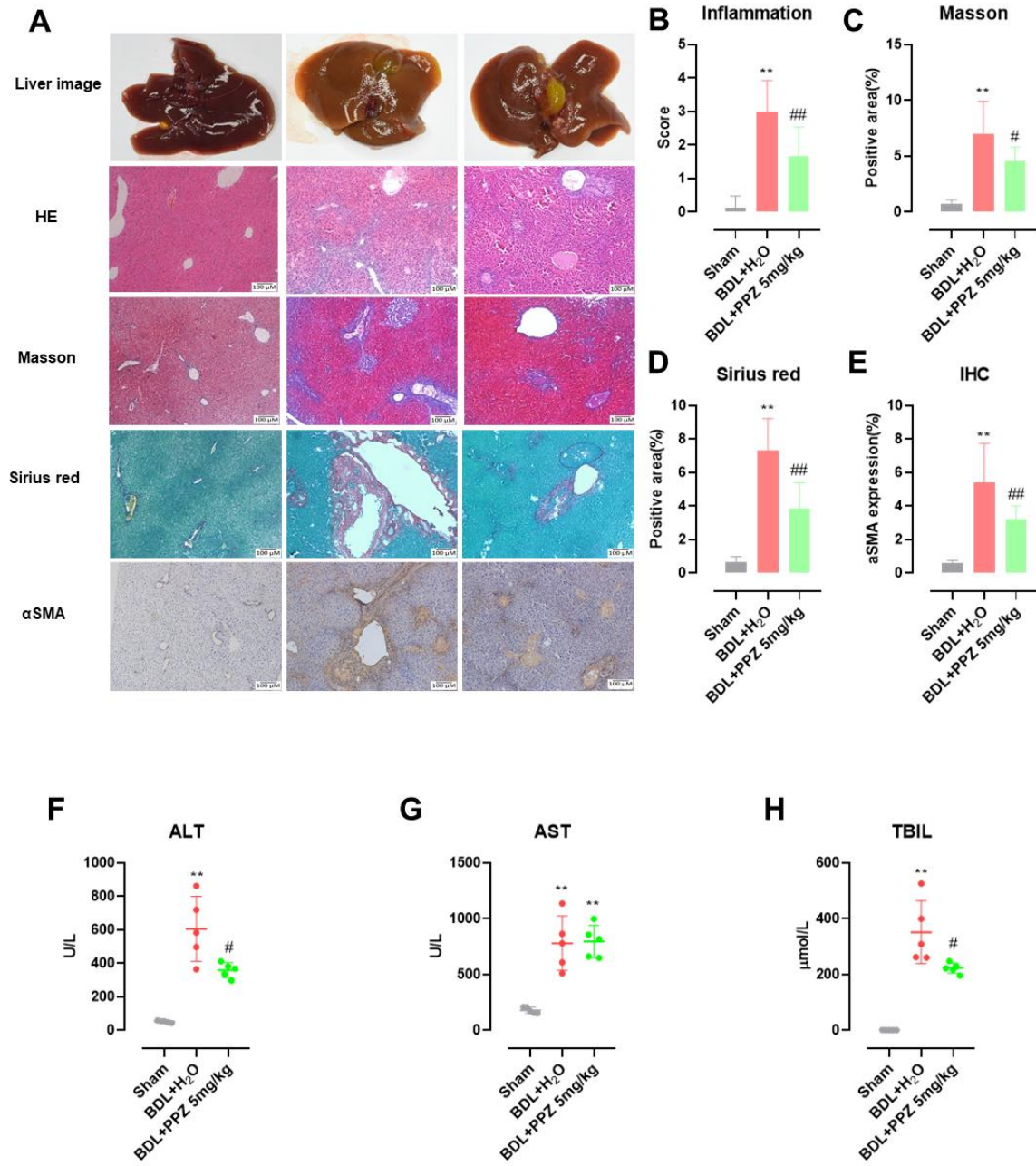
inflammation was semi-quantitatively assessed (B) and quantitative assessment (% of total area) is given for Masson staining (C), Sirius red staining (D) and IHC for α SMA (E) is presented. From serum biochemistry, levels of ALT (F), AST (G), alkaline phosphatase (H) and total bilirubin (I) are given. For rt-qPCR, mRNA expressions of pro-fibrotic markers, TIMP1 (J) and PDGFB (K), are reported. (n=5-7; *, p <0.05; **, p <0.01, compared to control; #, p <0.05; ##, p <0.01, compared to DDC + H₂O; t-test, ANOVA, post-hoc LSD or Tukey)

4.8 Pantoprazole prevents liver fibrosis in the BDL model of acute cholestasis

To further evaluate therapeutic effects of PPZ (5 mg/Kg) for cholestatic liver fibrosis, we performed BDL for 2 weeks as a mouse model for acute cholestasis. We found that BDL mice presented a general pale and tough appearance of liver compared to the sham group, but PPZ treatment improved liver general appearance for BDL mice (Figure 16A). H&E staining showed a damaged liver structure in BDL mice, while PPZ administration improved liver morphology compared with BDL mice (Figure 16A and B). Moreover, Sirius red staining and Masson staining were performed to analyze liver fibrosis degree in mice. This showed that severe liver fibrosis was developed in BDL mice compared to the sham group, while PPZ treatment significantly ameliorated liver fibrosis (Figure 16A, C and D). In immunohistochemistry, BDL mice demonstrated significant upregulation of the fibrotic marker α SMA compared to the sham group, which was also down-regulated significantly by PPZ (Figure 16A and E). Next, serum biochemistry analysis showed that ALT and TBIL were significantly increased in BDL mice compared to sham-treated animals but were significantly reduced when PPZ was applied (Figure 16F and H). To further verify the antifibrotic effect of PPZ for cholestatic liver

fibrosis, we measured the mRNA expression of pro-fibrotic markers, including α SMA (encoded by ACTA2), TGF β 1, PDGFB, LOX, COL1 α 1 and TIMP1. Our results showed that PPZ significantly inhibited the BDL-induced increases in the mRNA expression of these markers (Figure 16I-N).

Taken together, these *in vivo* data suggest that PPZ improves liver damage and liver inflammation in the BDL mouse model of acute cholestasis and ameliorates activation of pro-fibrogenic pathways and liver fibrosis.



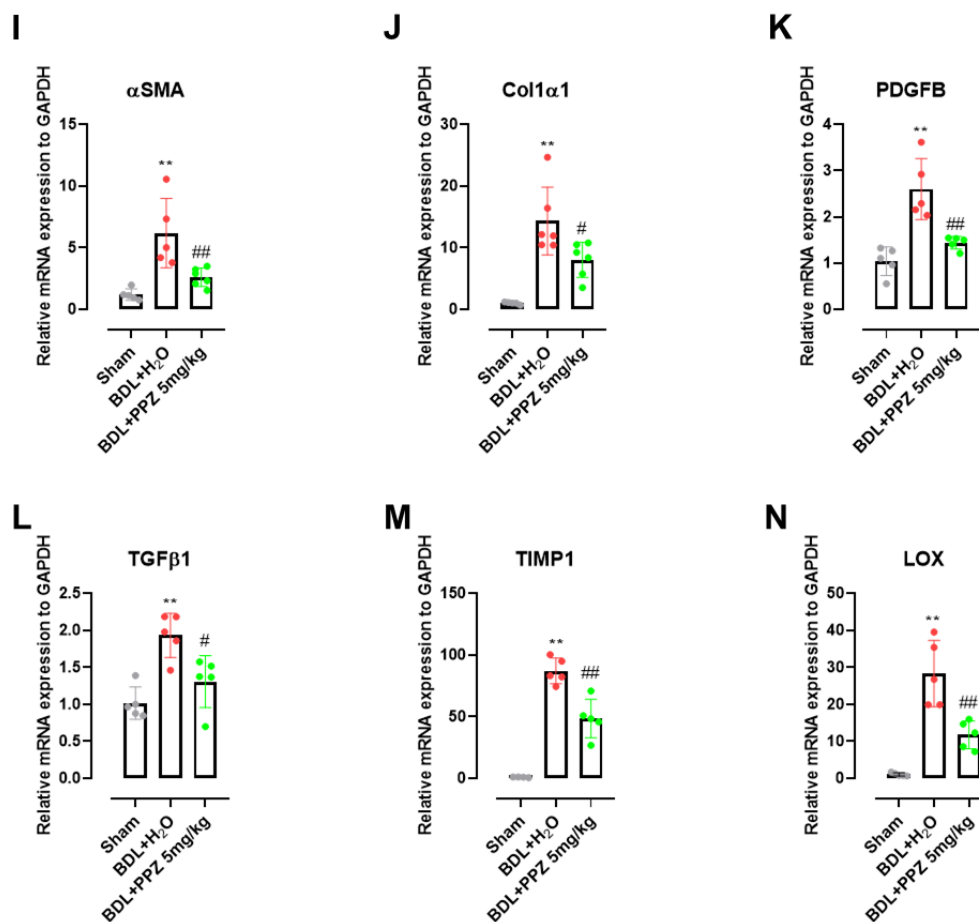


Figure 16. PPZ ameliorates BDL-induced cholestatic liver fibrosis in mice.

C57BL/6 male mice aged 4-6 weeks were performed with sham or BDL and were administered with H₂O as control or PPZ at 5 mg/kg, twice a day, i.p., for 2 weeks. Representative images for general macroscopic appearance, H&E, Masson staining, Sirius red staining and IHC for α SMA are given in (A). Liver inflammation was semi-quantitatively assessed (B) and quantitative assessment (% of total area) is given for Masson staining (C), Sirius red staining (D) and IHC for α SMA (E) is presented. From serum biochemistry, levels of ALT (F), AST (G) and total bilirubin (H) are given. For rt-qPCR, mRNA expressions of pro-fibrotic markers, α SMA (I), col1 α 1 (J), PDGFB (K), TGF β 1 (L), TIMP1 (M) and LOX (M), are reported. (n=5-7; *, p <0.05; **, p <0.01, compared to control; #, p <0.05; ##, p <0.01, compared to DDC + H₂O; t-test, ANOVA, post-hoc LSD or Tukey)

5. Discussion

Accumulation of toxic bile salts in chronic cholestatic liver disease is believed to drive liver fibrosis. However, underlying mechanisms for bile salt-induced fibrogenesis remain incompletely characterized. In this project, we aimed to further investigate into the role of bile salts in cholestatic liver fibrosis and underlying mechanisms.

We have previously shown that a humanized bile salt pool induced by GCDC feeding in a mouse model of hepatocellular cholestasis was a prerequisite for the induction of liver fibrosis³⁰. Therefore, we further explored profibrotic properties of a humanized bile salt pool in another, independent mouse model of cholestasis (BDL) and in a model of gross liver fibrosis without cholestasis (CCl₄ mouse model). In our experiments, a humanized bile salt pool resulting from GCDC feeding could again be confirmed in our BDL (Figure 5) and CCl₄ experiments (Figure 6). Next, we found that GCDC feeding aggravated liver fibrosis in BDL mice (Figure 7). Furthermore, GCDC feeding demonstrated no promotion to liver damage, liver inflammation and cholestasis as showed by serum biochemistry (Figure 7). These results indicate that humanization of the bile salt pool by GCDC feeding specifically promotes fibrogenesis, without inducing additional liver damage. Pro-fibrotic effects were also found following humanization of the bile salt pool in CCl₄ (Figure 8).

Which mechanisms might translate the humanized bile salt pool into pro-fibrogenic signals? It has previously been reported that bile salts might directly induce proliferation and extracellular matrix deposition by HSC^{30,37}. We had observed, however, that GCDC, the predominant bile salt accumulating in chronic cholestatic liver disease in man, was less effective in activating HSCs compared to unconjugated CDC. This led us to reconsider the microenvironment in which HSCs

reside, the slightly acidic perisinusoidal space, as pH has been shown to be an important co-factor for bile salt-induced signaling in cholangiocytes⁴¹.

In the current study, we confirmed that GCDC, unlike CDC, was unable to activate LX2 cells in standard culture conditions (Figure 9). Subsequently, we could demonstrate that a slightly acidic extracellular pH (pH 7.3) was a prerequisite for GCDC-induced activation of LX2 (Figure 10). Acidic pHe led to enhanced intracellular bile salt accumulation and GCDC-induced α SMA expression and proliferation. Given the microenvironment of a slightly acidic pH in the perisinusoidal space, this observation is of potential pathophysiologic relevance. Since pHe in the portal blood stream can hardly be targeted therapeutically, we investigated into the effects of modifying intracellular pH in HSC. PPZ as a model PPI was indeed able to lower intracellular pH in LX2 cells and we could attribute this effect to inhibition of NHE (Figure 11A). To the best of our knowledge, this is the first report to show inhibition of NHE by PPZ in HSCs. Lower pHi in LX2 led to a reduction in bile salt accumulation and inhibited bile salt-induced α SMA- and collagen1 α 1-expression as well as bile salt-induced proliferation (Figure 11 and 12). These observations could be reproduced when alternative PPIs were used, namely the NHE inhibitor amiloride and the vacuolar-ATPase inhibitor bafilomycin A1 (Figure 13-14). Lastly, PPZ was tested in mouse models of chronic and acute cholestatic liver fibrosis. PPZ did not alter cholestasis, liver damage or inflammation in the DDC-mouse model but ameliorated liver fibrosis, indicative of a specific antifibrotic effect of PPZ (Figure 15). Furthermore, PPZ significantly improved liver damage, inflammation and liver fibrosis in the BDL-mouse model (Figure 16).

Potentially (passive entry of bile salts) is a prerequisite for HSC activation. Bile salts can enter cells in the form of protonated, apolar bile acids, which is critically determined by pH_e and bile acid pK_a , the latter being dependent on bile salt conjugation ($pK_a \sim 4.2$ for GCDG compared to ~ 4.5 for CDC). Our findings of pH-dependent bile salt entry into HSC are in line with previous studies in cholangiocytes⁴¹. We furthermore showed that pharmacologically addressing pH_i in HSC may serve to prevent bile salt accumulation and HSC activation in chronic cholestasis. How would lowering the pH_i influence intracellular bile salt accumulation? Upon passive entry of a protonated bile acid into the cell, the acid would be deprotonated to the corresponding bile salt due to the more alkaline pH present in the intracellular compartment. The bile salt, carrying an electronic charge, would then be unable to passively exit the cell and would be 'trapped' intracellularly. Over time, this would lead to accumulation of bile salts within the cells.

It is well established that bile salts as hydrophobic substances can passively enter cells as bile acids, i.e., when being protonated and apolar. In presence of an active bile salt uptake system, however, passive entry would most likely be of minor relevance. NTCP as the major bile salt uptake transporter in hepatocytes has been speculated to be present in HSCs³⁹, but recent evidence suggests that its expression might not be associated with relevant bile salt uptake⁴⁰. To further exclude a relevant contribution of active bile salt uptake to bile salt-induced activation in LX2, we applied inhibitors for NTCP and OATPs, myrcludex B and sulfasalazine, respectively. We found that inhibition of both bile salt uptake transporters was without effect on (G)CDC-induced LX2 activation, suggesting a predominant role for passive bile acid entry in our system.

Another means of LX2 activation, independent of passive bile acid entry, would be activation of membrane receptors. The best characterized bile acid receptor on HSCs, however, TGR5, is primarily expressed in activated HSCs, but not silent HSCs^{57,58}. Furthermore, TGR5 has a very low affinity for (G)CDC⁵⁷. Thus, the role of TGR5 for (G)CDC-induced activation of dormant HSC seems negligible.

In the recent study, we found PPZ to lower intracellular pH in LX2 cells, likely by inhibition of NHE. This was associated with a decrease in intracellular bile salt accumulation and subsequent activation of LX2. PPIs are known however, to have effects beyond proton pump inhibition, e.g., anti-inflammatory and anti-oxidative properties^{59,60}. Thus, some other, pleiotropic effects of PPZ may have caused the observed effects on HSC activation other than alteration of pH-dependent bile salt uptake. To exclude a solely anti-fibrotic class effect of PPIs, we tested additional inhibitors, chemically different from PPZ. With both the NHE inhibitor amiloride and the v-H⁺-ATPase inhibitor bafilomycin A1, pHi was demonstrated to be lowered and for both inhibitors, this, too, was associated with reduced bile salt accumulation and activation of LX2. This supports our view, that proton-pump-inhibition prevents LX2 activation specifically by pHi-alteration and inhibition of intracellular bile salt accumulation. Furthermore, we tested the effect of PPZ, amiloride and bafilomycin A1 on TGFβ-induced LX2 activation. While bafilomycin A1 indeed was antifibrotic in this setting, PPZ was less effective in lowering TGFβ-induced LX2 activation than in lowering bile salt-induced LX2 activation and amiloride was without antifibrotic properties upon TGFβ-stimulation. Thus, while we cannot completely exclude additional, pleiotropic effects of PPZ and other PPIs, part of their anti-fibrotic effects in our systems seem indeed to be attributable to pHi lowering and prevention of bile salt entry.

To translate our findings into an *in vivo* system, the DDC-diet and BDL mouse models were applied. The dosage of PPZ applied in humans ranges from approximately 0.66 mg/kg body weight in long term care (40 mg qd for a 60kg person) up to 4 mg/kg in acute upper GI bleeding (10 mg per hour for a 60kg person). Given the increased metabolism in mice, translational mouse models are usually applied with higher doses compared to humans. Thus, the 5 mg/kg body weight applied here, are well within a standard therapeutic range. Our report is the first one to indicate a therapeutic effect of PPZ on liver fibrosis in mice. Noteworthy, in DDC-diet mouse model, PPZ had little or no effect on the cholestatic phenotype, liver inflammation or liver cell damage, but specifically prevented HSC expansion (as determined by IHC for α SMA) and liver fibrosis and in BDL mouse model, PPZ not only significantly improved liver inflammation or liver cell, but liver fibrosis degree. Our results are in line with a recent report by Zhen-ning Lu *et al*, who demonstrated an anti-fibrotic effect of PPZ in bile duct ligation rats ⁶¹. They attributed this finding to increased YAP degradation, while our results suggest an additional mode of action via pHi alteration in HSC. However, due to high dosage of PPZ used *in vitro* (100-300 μ M) and *in vivo* (150 mg/kg) ⁶¹, these results need to be interpreted with caution. In fact, these doses had previously been associated with pro-fibrogenic rather than therapeutic effects, when Assalin H.B *et al*. found that PPZ induced liver fibrosis in mice (150 mg/kg for 60 days) ⁶².

In patients with liver cirrhosis, PPI intake has recently been associated with an increased probability of decompensation in a retrospective cohort ⁶³. This possibly can be explained by an increased sensitivity towards infections in this highly susceptible cohort and does not necessarily exclude beneficial effects on fibrogenesis, when PPI are

applied in early stages of disease. Furthermore, our results suggest that other pHi modulating agents for specific uptake by HSCs might deserve further development, which might come without the increased risk of infection which is associated with PPZ administration.

5.1 Conclusion

In conclusion, firstly, we provide further evidence that the bile salt composition greatly impacts the development in chronic liver disease both in cholestatic and non-cholestatic etiologies. Secondly, we have shown that bile salts can directly activate HSCs to induce their proliferation and collagen deposition. We furthermore could demonstrate for the first time that pHe critically modulates bile salt-induced HSC activation, highlighting the role of pHe as part of the microenvironment of HSCs in the Space of Disse. Lastly, we could establish pHi modulation by PPIs as a method to inhibit bile salt entry into HSC and bile salt-induced HSC activation. At the last, we showed that pantoprazole significantly ameliorates acute and chronic cholestatic liver fibrosis.

5.2 Outlook

Bile salt-induced HSC activation in cholestatic and other liver diseases may depend on the slightly acidic pH known to be present in the perisinusoidal space. To further solidify our observation, we are currently transferring our experiments to additional *in vitro* models, using alternative HSC cell lines as well as primary HSC. The current data established a novel potential therapeutic strategy for targeting liver fibrosis by modulating pHi in HSCs. This may be possible with cell-type- targeted drugs in the near future and deserves further *in vitro* and *in vivo* exploration.

References

1. Trefts E, Gannon M, Wasserman DH. The liver. *Curr Biol*. Nov 6 2017;27(21):R1147-r1151. doi:10.1016/j.cub.2017.09.019
2. Tsochatzis EA, Bosch J, Burroughs AK. Liver cirrhosis. *Lancet*. May 17 2014;383(9930):1749-61. doi:10.1016/s0140-6736(14)60121-5
3. Ginès P, Krag A, Abraldes JG, Solà E, Fabrellas N, Kamath PS. Liver cirrhosis. *Lancet*. Oct 9 2021;398(10308):1359-1376. doi:10.1016/s0140-6736(21)01374-x
4. Asrani SK, Devarbhavi H, Eaton J, Kamath PS. Burden of liver diseases in the world. *J Hepatol*. Jan 2019;70(1):151-171. doi:10.1016/j.jhep.2018.09.014
5. Meirelles Júnior RF, Salvalaggio P, Rezende MB, et al. Liver transplantation: history, outcomes and perspectives. *Einstein (Sao Paulo)*. Jan-Mar 2015;13(1):149-52. doi:10.1590/s1679-45082015rw3164
6. The global, regional, and national burden of cirrhosis by cause in 195 countries and territories, 1990-2017: a systematic analysis for the Global Burden of Disease Study 2017. *Lancet Gastroenterol Hepatol*. Mar 2020;5(3):245-266. doi:10.1016/s2468-1253(19)30349-8
7. Lu L. Guidelines for the Management of Cholestatic Liver Diseases (2021). *J Clin Transl Hepatol*. Aug 28 2022;10(4):757-769. doi:10.14218/jcth.2022.00147
8. Hasegawa S, Yoneda M, Kurita Y, et al. Cholestatic Liver Disease: Current Treatment Strategies and New Therapeutic Agents. *Drugs*. Jul 2021;81(10):1181-1192. doi:10.1007/s40265-021-01545-7
9. Sebode M, Kloppenburg A, Aigner A, Lohse AW, Schramm C, Linder R. Population-based study of autoimmune hepatitis and primary biliary cholangitis in Germany: rising prevalences based on ICD codes, yet deficits in medical treatment. *Z Gastroenterol*. May 2020;58(5):431-438. Populationsbasierte Analyse von autoimmuner Hepatitis und primär biliärer Cholangitis in Deutschland: ansteigende Prävalenzen basierend auf ICD Codes, aber Defizite bei der medikamentösen Therapie. doi:10.1055/a-1135-9306
10. El-Guindi MA, Sira MM, Hussein MH, Ehsan NA, Elsheikh NM. Hepatic immunohistochemistry of bile transporters in progressive familial intrahepatic cholestasis. *Ann Hepatol*. Mar-Apr 2016;15(2):222-9. doi:10.5604/16652681.1193718
11. Hirschfield GM, Heathcote EJ, Gershwin ME. Pathogenesis of cholestatic liver disease and therapeutic approaches. *Gastroenterology*. Nov 2010;139(5):1481-96. doi:10.1053/j.gastro.2010.09.004
12. Greim H, Trülzsch D, Czygan P, et al. Mechanism of cholestasis. 6. Bile acids in human livers with or without biliary obstruction. *Gastroenterology*. Nov 1972;63(5):846-50.
13. Greim H, Trülzsch D, Roboz J, et al. Mechanism of cholestasis. 5. Bile acids in normal rat livers and in those after bile duct ligation. *Gastroenterology*. Nov 1972;63(5):837-45.
14. Murphy GM, Ross A, Billing BH. Serum bile acids in primary biliary cirrhosis. *Gut*. Mar 1972;13(3):201-6. doi:10.1136/gut.13.3.201
15. Dyrszka H, Salen G, Zaki FG, Chen T, Mosbach EH. Hepatic toxicity in the rhesus monkey treated with chenodeoxycholic acid for 6 months: biochemical and ultrastructural studies. *Gastroenterology*. Jan 1976;70(1):93-104.

16. Malhi H, Gores GJ. Cellular and molecular mechanisms of liver injury. *Gastroenterology*. May 2008;134(6):1641-54. doi:10.1053/j.gastro.2008.03.002
17. Friedman SL. Mechanisms of hepatic fibrogenesis. *Gastroenterology*. May 2008;134(6):1655-69. doi:10.1053/j.gastro.2008.03.003
18. Guicciardi ME, Gores GJ. Bile acid-mediated hepatocyte apoptosis and cholestatic liver disease. *Dig Liver Dis*. Jun 2002;34(6):387-92. doi:10.1016/s1590-8658(02)80033-0
19. Fickert P, Wagner M. Biliary bile acids in hepatobiliary injury - What is the link? *J Hepatol*. Sep 2017;67(3):619-631. doi:10.1016/j.jhep.2017.04.026
20. Patel T, Bronk SF, Gores GJ. Increases of intracellular magnesium promote glycodeoxycholate-induced apoptosis in rat hepatocytes. *J Clin Invest*. Dec 1994;94(6):2183-92. doi:10.1172/jci117579
21. Faubion WA, Guicciardi ME, Miyoshi H, et al. Toxic bile salts induce rodent hepatocyte apoptosis via direct activation of Fas. *J Clin Invest*. Jan 1999;103(1):137-45. doi:10.1172/jci4765
22. Reinehr R, Graf D, Häussinger D. Bile salt-induced hepatocyte apoptosis involves epidermal growth factor receptor-dependent CD95 tyrosine phosphorylation. *Gastroenterology*. Sep 2003;125(3):839-53. doi:10.1016/s0016-5085(03)01055-2
23. Reinehr R, Becker S, Keitel V, Eberle A, Grether-Beck S, Häussinger D. Bile salt-induced apoptosis involves NADPH oxidase isoform activation. *Gastroenterology*. Dec 2005;129(6):2009-31. doi:10.1053/j.gastro.2005.09.023
24. Rust C, Wild N, Bernt C, Vennegeerts T, Wimmer R, Beuers U. Bile acid-induced apoptosis in hepatocytes is caspase-6-dependent. *J Biol Chem*. Jan 30 2009;284(5):2908-2916. doi:10.1074/jbc.M804585200
25. Hohenester S, Gates A, Wimmer R, et al. Phosphatidylinositol-3-kinase p110 γ contributes to bile salt-induced apoptosis in primary rat hepatocytes and human hepatoma cells. *J Hepatol*. Nov 2010;53(5):918-26. doi:10.1016/j.jhep.2010.05.015
26. Canbay A, Taimr P, Torok N, Higuchi H, Friedman S, Gores GJ. Apoptotic body engulfment by a human stellate cell line is profibrogenic. *Lab Invest*. May 2003;83(5):655-63. doi:10.1097/01.lab.0000069036.63405.5c
27. Zhan SS, Jiang JX, Wu J, et al. Phagocytosis of apoptotic bodies by hepatic stellate cells induces NADPH oxidase and is associated with liver fibrosis in vivo. *Hepatology*. Mar 2006;43(3):435-43. doi:10.1002/hep.21093
28. Watanabe A, Hashmi A, Gomes DA, et al. Apoptotic hepatocyte DNA inhibits hepatic stellate cell chemotaxis via toll-like receptor 9. *Hepatology*. Nov 2007;46(5):1509-18. doi:10.1002/hep.21867
29. Myung SJ, Yoon JH, Gwak GY, et al. Bile acid-mediated thrombospondin-1 induction in hepatocytes leads to transforming growth factor-beta-dependent hepatic stellate cell activation. *Biochem Biophys Res Commun*. Feb 23 2007;353(4):1091-6. doi:10.1016/j.bbrc.2006.12.157
30. Hohenester S, Kanitz V, Kremer AE, et al. Glycochenodeoxycholate Promotes Liver Fibrosis in Mice with Hepatocellular Cholestasis. *Cells*. Jan 23 2020;9(2)doi:10.3390/cells9020281

31. Wang R, Salem M, Yousef IM, et al. Targeted inactivation of sister of P-glycoprotein gene (spgp) in mice results in nonprogressive but persistent intrahepatic cholestasis. *Proc Natl Acad Sci U S A*. Feb 13 2001;98(4):2011-6. doi:10.1073/pnas.98.4.2011
32. Pinzani M, Luong TV. Pathogenesis of biliary fibrosis. *Biochim Biophys Acta Mol Basis Dis*. Apr 2018;1864(4 Pt B):1279-1283. doi:10.1016/j.bbadis.2017.07.026
33. Bertolini A, Fiorotto R, Strazzabosco M. Bile acids and their receptors: modulators and therapeutic targets in liver inflammation. *Semin Immunopathol*. Jul 2022;44(4):547-564. doi:10.1007/s00281-022-00935-7
34. Brady LM, Beno DW, Davis BH. Bile acid stimulation of early growth response gene and mitogen-activated protein kinase is protein kinase C-dependent. *Biochem J*. Jun 15 1996;316 (Pt 3)(Pt 3):765-9. doi:10.1042/bj3160765
35. Svegliati-Baroni G, Ridolfi F, Hannivoort R, et al. Bile acids induce hepatic stellate cell proliferation via activation of the epidermal growth factor receptor. *Gastroenterology*. Apr 2005;128(4):1042-55. doi:10.1053/j.gastro.2005.01.007
36. Dilger K, Hohenester S, Winkler-Budenhofer U, et al. Effect of ursodeoxycholic acid on bile acid profiles and intestinal detoxification machinery in primary biliary cirrhosis and health. *J Hepatol*. Jul 2012;57(1):133-40. doi:10.1016/j.jhep.2012.02.014
37. Zimny S, Koob D, Li J, et al. Hydrophobic Bile Salts Induce Pro-Fibrogenic Proliferation of Hepatic Stellate Cells through PI3K p110 Alpha Signaling. *Cells*. Jul 29 2022;11(15)doi:10.3390/cells11152344
38. Jani M, Beéry E, Heslop T, et al. Kinetic characterization of bile salt transport by human NTCP (SLC10A1). *Toxicol In Vitro*. Feb 2018;46:189-193. doi:10.1016/j.tiv.2017.10.012
39. Salhab A, Amer J, Lu Y, Safadi R. Sodium(+)/taurocholate cotransporting polypeptide as target therapy for liver fibrosis. *Gut*. Jul 2022;71(7):1373-1385. doi:10.1136/gutjnl-2020-323345
40. Kunst RF, Paulusma CC, van de Graaf SFJ. Insufficient evidence for NTCP activity in stellate cells. *Gut*. Dec 15 2021;71(10):2140-1. doi:10.1136/gutjnl-2021-326452
41. Hohenester S, Wenniger LM, Paulusma CC, et al. A biliary HCO₃⁻ umbrella constitutes a protective mechanism against bile acid-induced injury in human cholangiocytes. *Hepatology*. Jan 2012;55(1):173-83. doi:10.1002/hep.24691
42. Beuers U, Hohenester S, de Buy Wenniger LJ, Kremer AE, Jansen PL, Elferink RP. The biliary HCO₃⁻ umbrella: a unifying hypothesis on pathogenetic and therapeutic aspects of fibrosing cholangiopathies. *Hepatology*. Oct 2010;52(4):1489-96. doi:10.1002/hep.23810
43. Ichikawa M, Kato Y, Miyauchi S, et al. Effect of perfusate pH on the influx of 5'-5'-dimethyl-oxazolidine-2,4-dione and dissociation of epidermal growth factor from the cell-surface receptor: the existence of the proton diffusion barrier in the Disse space. *J Hepatol*. Feb 1994;20(2):190-200. doi:10.1016/s0168-8278(05)80057-1
44. Kang YB, Rawat S, Cirillo J, Bouchard M, Noh HM. Layered long-term co-culture of hepatocytes and endothelial cells on a transwell membrane: toward engineering the liver sinusoid. *Biofabrication*. Dec 2013;5(4):045008. doi:10.1088/1758-5082/5/4/045008

45. Reiter FP, Ye L, Ofner A, et al. p70 Ribosomal Protein S6 Kinase Is a Checkpoint of Human Hepatic Stellate Cell Activation and Liver Fibrosis in Mice. *Cell Mol Gastroenterol Hepatol*. 2022;13(1):95-112. doi:10.1016/j.jcmgh.2021.09.001
46. Franko A, Kovarova M, Feil S, et al. cGMP-dependent protein kinase I (cGKI) modulates human hepatic stellate cell activation. *Metabolism*. Nov 2018;88:22-30. doi:10.1016/j.metabol.2018.09.001
47. da Silva CM, Caetano FH, Pereira FDC, Morales MAM, Sakane KK, Moraes KCM. Cellular and molecular effects of *Baccharis dracunculifolia* D.C. and *Plectranthus barbatus* Andrews medicinal plant extracts on retinoid metabolism in the human hepatic stellate cell LX-2. *BMC Complement Altern Med*. Aug 22 2019;19(1):222. doi:10.1186/s12906-019-2591-8
48. Carson JP, Robinson MW, Ramm GA, Gobert GN. RNA sequencing of LX-2 cells treated with TGF- β 1 identifies genes associated with hepatic stellate cell activation. *Mol Biol Rep*. Dec 2021;48(12):7677-7688. doi:10.1007/s11033-021-06774-3
49. Ebata S, Muto S, Okada K, et al. Aldosterone activates Na⁺/H⁺ exchange in vascular smooth muscle cells by nongenomic and genomic mechanisms. *Kidney Int*. Oct 1999;56(4):1400-12. doi:10.1046/j.1523-1755.1999.00674.x
50. Miyoshi H, Rust C, Roberts PJ, Burgart LJ, Gores GJ. Hepatocyte apoptosis after bile duct ligation in the mouse involves Fas. *Gastroenterology*. Sep 1999;117(3):669-77. doi:10.1016/s0016-5085(99)70461-0
51. Donkers JM, Appelman MD, van de Graaf SFJ. Mechanistic insights into the inhibition of NTCP by myrcludex B. *JHEP Rep*. Oct 2019;1(4):278-285. doi:10.1016/j.jhepr.2019.07.006
52. Karlgren M, Vildhede A, Norinder U, et al. Classification of inhibitors of hepatic organic anion transporting polypeptides (OATPs): influence of protein expression on drug-drug interactions. *J Med Chem*. May 24 2012;55(10):4740-63. doi:10.1021/jm300212s
53. Di Sario A, Svegliati Baroni G, Bendia E, et al. Intracellular pH regulation and Na⁺/H⁺ exchange activity in human hepatic stellate cells: effect of platelet-derived growth factor, insulin-like growth factor 1 and insulin. *J Hepatol*. Mar 2001;34(3):378-85. doi:10.1016/s0168-8278(00)00062-3
54. Di Sario A, Baroni GS, Bendia E, et al. Characterization of ion transport mechanisms regulating intracellular pH in hepatic stellate cells. *Am J Physiol*. Jul 1997;273(1 Pt 1):G39-48. doi:10.1152/ajpgi.1997.273.1.G39
55. Benedetti A, Di Sario A, Casini A, et al. Inhibition of the NA(+)/H(+) exchanger reduces rat hepatic stellate cell activity and liver fibrosis: an in vitro and in vivo study. *Gastroenterology*. Feb 2001;120(2):545-56. doi:10.1053/gast.2001.21203
56. Marrone G, De Chiara F, Böttcher K, et al. The adenosine monophosphate-activated protein kinase-vacuolar adenosine triphosphatase-pH axis: A key regulator of the profibrogenic phenotype of human hepatic stellate cells. *Hepatology*. Sep 2018;68(3):1140-1153. doi:10.1002/hep.30029
57. Xie G, Jiang R, Wang X, et al. Conjugated secondary 12 α -hydroxylated bile acids promote liver fibrogenesis. *EBioMedicine*. Apr 2021;66:103290. doi:10.1016/j.ebiom.2021.103290

58. Keitel V, Donner M, Winandy S, Kubitz R, Häussinger D. Expression and function of the bile acid receptor TGR5 in Kupffer cells. *Biochem Biophys Res Commun*. Jul 18 2008;372(1):78-84. doi:10.1016/j.bbrc.2008.04.171
59. De Milito A, Iessi E, Logozzi M, et al. Proton pump inhibitors induce apoptosis of human B-cell tumors through a caspase-independent mechanism involving reactive oxygen species. *Cancer Res*. Jun 1 2007;67(11):5408-17. doi:10.1158/0008-5472.Can-06-4095
60. Kedika RR, Souza RF, Spechler SJ. Potential anti-inflammatory effects of proton pump inhibitors: a review and discussion of the clinical implications. *Dig Dis Sci*. Nov 2009;54(11):2312-7. doi:10.1007/s10620-009-0951-9
61. Lu ZN, Niu WX, Zhang N, et al. Pantoprazole ameliorates liver fibrosis and suppresses hepatic stellate cell activation in bile duct ligation rats by promoting YAP degradation. *Acta Pharmacol Sin*. Nov 2021;42(11):1808-1820. doi:10.1038/s41401-021-00754-w
62. Assalin HB, De Almeida KCG, Guadagnini D, et al. Proton Pump Inhibitor Pantoprazole Modulates Intestinal Microbiota and Induces TLR4 Signaling and Fibrosis in Mouse Liver. *Int J Mol Sci*. Nov 9 2022;23(22)doi:10.3390/ijms232213766
63. Mahmud N, Serper M, Taddei TH, Kaplan DE. The Association Between Proton Pump Inhibitor Exposure and Key Liver-Related Outcomes in Patients With Cirrhosis: A Veterans Affairs Cohort Study. *Gastroenterology*. Jul 2022;163(1):257-269.e6. doi:10.1053/j.gastro.2022.03.052

Acknowledgements

It is still unbelievable that I am typing here to put an end for my dissertation in Med 2, for my MD study in Munich, also, for this 3-year amazing journey in my life.

I can't express more appreciation and gratitude to my supervisor, PD Dr. Dr. Simon Hohenester, who provides me this opportunity to pursue my MD degree in his scientific group. Dr Hohenester is absolutely a professional and excellent supervisor with great passion and sharp brain both in science and clinic. During my study, with great expertise and rigorous attitude, he led me to explore interesting scientific questions and instructed me to make manuscript and dissertation. Besides, he gave me a lot of space to think how to promote our project and how to make it better, which is not merely following what he says, but cultivating and exercising my scientific mindset, from which I definitely benefit! Also, I want to express my deep and sincere gratitude to Prof. Biguang Tuo, who has been immensely supporting me in my career and life.

I would like to thank my colleagues in Med 2 for their kindness, patience and cooperation during my stay here. They are Ralf, Renate, Dennis, Dr. Zimny and Prof. Denk. Additionally, I want to thank my senior LMU-mate, Dr. Liangtao Ye, who really helped and taught me a lot in my scientific career and my life. I was inspired and stimulated by him greatly, my precious friend! Furthermore, I would like to thank the Chinese Scholarship Council (CSC) for its financial support for my study and life in Munich!

At the last, I want to thank my parents. They love me so deeply and me as well. I hope that we all have our wonderful time and live our lovely life!

Affidavit



LUDWIG-
MAXIMILIANS-
UNIVERSITÄT
MÜNCHEN

Promotionsbüro
Medizinische Fakultät



Affidavit

Li, Jingguo

Surname, first name

Street

Zip code, town, country

I hereby declare, that the submitted thesis entitled:

The role of bile salts in cholestatic liver fibrosis
.....

is my own work. I have only used the sources indicated and have not made unauthorised use of services of a third party. Where the work of others has been quoted or reproduced, the source is always given.

I further declare that the dissertation presented here has not been submitted in the same or similar form to any other institution for the purpose of obtaining an academic degree.

_Munich 15,05,2024_____
place, date

_____Jingguo Li_____
Signature doctoral candidate

List of publications

Publications:

Zimny, S., Koob, D., Li, J., Wimmer, R., Schiergens, T., Nagel, J., Reiter, F. P., Denk, G., Hohenester, S. (2022). Hydrophobic Bile Salts Induce Pro-Fibrogenic Proliferation of Hepatic Stellate Cells through PI3K p110 Alpha Signaling. *Cells*, 11(15), 2344.
<https://doi.org/10.3390/cells11152344>

Li, J., Tuo, B. (2021). Current and Emerging Approaches for Hepatic Fibrosis Treatment. *Gastroenterology research and practice*, 2021, 6612892. <https://doi.org/10.1155/2021/6612892>

Li, J., Yang, Z., Tuo, B. (2019). Role of OCT1 in hepatocellular carcinoma. *OncoTargets and therapy*, 12, 6013–6022.
<https://doi.org/10.2147/OTT.S212088>

Abstracts:

Jingguo Li, Sebastian Zimny, Shun Yao, Dennis Koob, Hai Jin, Ralf Wimmer, Gerald Denk, Biguang Tuo, Simon Hohenester. (2023). Mo1564 BILE SALT-INDUCED ACTIVATION OF HEPATIC STELLATE CELLS DEPENDS ON ACIDIC EXTRACELLULAR PH AND IS AMELIORATED BY INHIBITING INTRACELLULAR PROTON PUMPS. *Gastroenterology*. 164. S-1372. 10.1016/S0016-5085(23)04198-7.

Jingguo Li, Sebastian Zimny, Shun Yao, Dennis Koob, Hai Jin, Ralf Wimmer, Gerald Denk, Biguang Tuo, Simon Hohenester. (2023).

Composition of the bile salt pool critically modulates liver fibrosis-towards humanization of murine models of liver disease. *Journal of Hepatology*. 78. S329-S330. 10.1016/S0168-8278(23)00946-7.

Dennis Koob, Judith Nagel, Sebastian Zimny, **Jingguo Li**, Renate Artmann, Ralf Wimmer, Gerald Denk, Martin Roderfeld, Elke Roeb, Hans Zischka, Simon Hohenester. (2022). Copper accumulation in chronic cholestatic disease augments liver damage by impairment of mitochondrial function. *Journal of Hepatology*. 77. S602-S603. 10.1016/S0168-8278(22)01522-7.

Dennis Koob, Judith Nagel, **Jingguo Li**, Sebastian Zimny, Ralf Wimmer, Gerald Denk, Martin Roderfeld, Elke Roeb, Svetlana Lutsenko, Hans Zischka, Simon Hohenester. (2023). Depletion of excess liver copper ameliorates liver damage in a mouse model of chronic cholestatic liver disease. *Journal of Hepatology*. 78. S417. 10.1016/S0168-8278(23)01090-5.